HHS Public Access

Author manuscript

Gene Ther. Author manuscript; available in PMC 2021 September 12.

Published in final edited form as:

Gene Ther. 2021 June ; 28(6): 373–390. doi:10.1038/s41434-021-00251-z.

Correction of X-CGD patient HSPCs by targeted *CYBB* cDNA insertion using CRISPR/Cas9 with 53BP1 inhibition for enhanced homology-directed repair

Colin L. Sweeney[1,*], **Mara Pavel-Dinu**[2,*], **Uimook Choi**[1], **Julie Brault**[1], **Taylor Liu**[1], **Sherry Koontz**[1], **Linhong Li**[3], **Narda Theobald**[1], **Janet Lee**[1], **Ezekiel A. Bello**[1], **Xiaolin Wu**[4], **Ronald J. Meis**[5], **Gary A. Dahl**[5], **Matthew H. Porteus**[2,†], **Harry L. Malech**[1], **Suk See De Ravin**[1,†]

[1]Genetic Immunotherapy Section, Laboratory of Clinical Immunology and Microbiology, National Institute of Allergy and Infectious Diseases, National Institutes of Health, Bethesda, MD 20892

[2]Department of Pediatrics, Stanford University School of Medicine, Stanford, CA 94305

[3]MaxCyte Inc., Gaithersburg, MD 20878

[4]Cancer Research Technology Program, Leidos Biomedical Research Inc., Frederick, MD 21701

[5]CELLSCRIPT, LLC, Madison, WI 53713.

Abstract

X-linked chronic granulomatous disease is an immunodeficiency characterized by defective production of microbicidal reactive oxygen species (ROS) by phagocytes. Causative mutations occur throughout the 13 exons and splice sites of the *CYBB* gene, resulting in loss of gp91^{phox} protein. Here we report gene correction by homology-directed repair in patient hematopoietic stem/progenitor cells (HSPCs) using CRISPR/Cas9 for targeted insertion of *CYBB* exon 1–13 or 2–13 cDNAs from adeno-associated virus donors at endogenous *CYBB* exon 1 or exon 2 sites. Targeted insertion of exon 1–13 cDNA did not restore physiologic gp91^{phox} levels, consistent with a requirement for intron 1 in *CYBB* expression. However, insertion of exon 2–13 cDNA fully restored gp91^{phox} and ROS production upon phagocyte differentiation. Addition of a woodchuck hepatitis virus post-transcriptional regulatory element did not further enhance gp91^{phox} expression in exon 2–13 corrected cells, indicating that retention of intron 1 was sufficient for optimal *CYBB* expression. Targeted correction was increased ~1.5-fold using i53 mRNA to transiently inhibit non-homologous end joining. Following engraftment in NSG mice, corrected HSPCs generated phagocytes with restored gp91^{phox} and ROS production. Our findings demonstrate the utility of

†**Corresponding authors:** Suk See De Ravin, MD, LCIM/NIAID/NIH; Bldg 10, Rm 5-3816, 10 Center Dr, MSC 1456, Bethesda, MD 20892-1456, sderavin@niaid.nih.gov, Tel: 301-496-6772, Fax: 301-402-4369, Matthew Porteus, MD, PhD, Lorry Lokey Stem Cell Research Building, G3045, 269 Campus Drive, MC 5462, Stanford, CA 94305, mporteus@stanford.edu, Tel: 650-725-6520.
*These authors contributed equally to this work

Compliance with ethical standards

Conflict of interest: L.L. was a full-time employee of MaxCyte Biosystems at the time of this study; R.J.M. and G.A.D. are full-time employees of CELLSCRIPT, LLC; M.H.P. holds equity in CRISPR Tx and Allogene Tx and serves on the Scientific Advisory Board for Allogene Tx; the remaining authors declare no conflict of interest.

tailoring donor design and targeting strategies to retain regulatory elements needed for optimal expression of the target gene.

Introduction

X-linked chronic granulomatous disease (X-CGD) is an immunodeficiency caused by mutations in the *CYBB* gene on the X-chromosome, predominantly affecting males due to their single allele. *CYBB* encodes the $gp91^{phox}$ (or NOX2) subunit of phagocyte NADPH oxidase, which is necessary for the production of reactive oxygen species (ROS) by neutrophils and other phagocytes for killing of select microbial organisms. Causative mutations can occur throughout the 13 exons or adjoining intronic splice sites of the >30-kb *CYBB* gene, resulting in defective or absent $gp91^{phox}$ protein expression and loss of ROS production [1]. X-CGD patients have recurring, life-threatening fungal and bacterial infections, hyper-inflammation, and granulomatous complications [2]. Allogeneic transplantation of $CD34^+$ hematopoietic stem/progenitor cells (HSPCs) can be curative for X-CGD, but graft-versus-host-disease remains a significant risk, and many patients lack a suitable matched donor. Autologous transplant of X-CGD patient HSPCs modified by random insertion of *CYBB* cDNA using retroviral vectors has demonstrated clinical benefit as salvage therapy for life-threatening infections, but has resulted in low levels of long-term gene marking in engrafted cells, as well as life-threatening myelodysplasia due to vector insertional mutagenesis [3, 4]. The use of constitutive promoters in these vectors for ectopic expression of $gp91^{phox}$ carries an additional potential risk of aberrant production of ROS in corrected HSPCs, which might alter stem cell function or impair long-term hematopoietic engraftment [5, 6]. To address these safety issues, a self-inactivating lentiviral vector was developed using a chimeric myeloid-specific promoter for phagocyte-restricted expression of *CYBB* cDNA [7], which is currently in use in clinical trials [8]; however, X-CGD patient HSPCs transduced to achieve ~1 copy of vector insert per cell exhibited $gp91^{phox}$ protein expression levels (in HSPC-derived phagocytes) that are only ~50% of levels detected in healthy donor controls, while physiologically normal levels of ROS production required multiple vector copies per cell [7], which could consequently increase insertional mutagenesis.

Targeted gene insertion or gene editing using site-specific nucleases, including CRISPR (clustered regularly interspaced short palindromic repeats)/Cas9 (CRISPR-associated 9) nuclease [9–11], zinc-finger nucleases (ZFNs) [12, 13], or transcription activator-like effector nucleases (TALENs) [14], has potential for gene therapy to maintain endogenous regulatory control of gene expression with a greatly reduced or absent risk of insertional mutagenesis. In these approaches, a DNA double-strand break (DSB) induced by the nuclease acts as a target for homology-directed repair (HDR) using a donor DNA template containing homologous sequences to those flanking the cut site. Due to the toxicity of double-stranded plasmid DNAs in transfections of primary cells [15, 16], adeno-associated virus (AAV) vectors packaged with serotype 6 capsid (AAV6) are commonly used for transduction of HSPCs [17–24] to deliver long donor DNA templates (with an upper size limit of ~4.7-kb for AAV vector packaging, including target site homologous sequences and ~0.3-kb for the required AAV inverted terminal repeats or ITRs), while single-stranded

oligodeoxynucleotides (ssODNs) have been used for gene repair or insertion of short donor templates (typically up to 100–200 nucleotides in length including homologous sequences) [22, 23, 25–30]. The efficiency of targeted insertion of a donor DNA template is dependent upon the choice of DSB repair pathways between HDR and non-homologous end joining (NHEJ) [31], a more error-prone repair pathway that functions without a homologous donor template and can instead result in the formation of indels (insertion or deletion mutations) at the DSB site. This choice of repair pathway appears to be cell type [32] and cell cycle dependent, with HDR normally restricted to S and G2 phases of the cell cycle [33], which poses an additional challenge for HDR-mediated genome editing in quiescent hematopoietic stem cells.

We previously described [20] a gene insertion approach for correction of X-CGD patient HSPCs using ZFNs targeting the “safe-harbor” AAVS1 locus [13] to mediate insertion of a codon-optimized full-length *CYBB* cDNA under the control of a constitutive promoter, using an AAV6 vector to deliver the donor DNA template for HDR. This safe-harbor targeted insertion strategy resulted in the constitutive expression of gp91^{phox} protein in HSPC-derived phagocytes at per-cell levels that were ~60% of levels in healthy donor controls, which restored ROS production in HSPC-derived phagocytes to per-cell levels ~90% of healthy controls, albeit with the potential risks associated with dysregulated constitutive gp91^{phox} expression mentioned above. As an alternative strategy for correction of a specific point mutation while maintaining normal physiological regulation of gene expression, we also described [27] the targeted repair of a C676T mutation in *CYBB* exon 7 in affected X-CGD patient HSPCs by CRISPR/Cas9 using a mutation-specific CRISPR single guide RNA (sgRNA) and a short ssODN donor template to correct the point mutation at this site by HDR. Gene correction in HSPCs by this approach resulted in the restoration of physiologically normal levels of gp91^{phox} protein expression and ROS production in HSPC-derived phagocytes, demonstrating an effective and efficient gene repair strategy for the cohort of patients that share this specific point mutation.

Successful HDR-mediated targeted insertion of a full-length cDNA at the corresponding endogenous locus has been described as a strategy for simultaneous correction of mutations occurring in multiple exons for other human genes, notably for *IL2RG* [21, 34] in HSPCs and *CD40LG* [35] in T cells. As a refinement of our *CYBB* targeting strategies to similarly correct the majority of X-CGD patient mutations while ensuring normal regulation and expression of gp91^{phox} protein at physiologic levels in corrected cells, we previously assessed [36] HDR-mediated targeted insertion of *CYBB* exon 1–13 or exon 2–13 cDNA constructs from plasmid DNA donor templates into exon 1 or exon 2 of the endogenous *CYBB* gene using either TALENs or CRISPR/Cas9 in induced pluripotent stem cells (iPSCs) as a model system. Surprisingly, we observed that targeted insertion of an intronless full-length exon 1–13 cDNA expression cassette into the start site of exon 1 in X-CGD iPSCs did not result in detectable gp91^{phox} expression or restoration of ROS production upon differentiation of iPSCs into granulocytes, presumably due to the elimination of a transcriptional regulatory element or another form of intron-mediated enhancement [37] necessary for expression from the *CYBB* promoter. In contrast, the targeted insertion of a *CYBB* exon 2–13 cDNA at the endogenous exon 2 site in X-CGD iPSCs (to retain the endogenous intron 1 in the gene transcript) resulted in near-normal levels of gp91^{phox}

expression and ROS production in differentiated granulocytes, without dysregulated expression in undifferentiated iPSCs, suggesting that elements present in *CYBB* intron 1 are necessary and sufficient for physiological regulation of *CYBB* promoter and cDNA expression.

Here we describe the further application of these strategies for efficient cDNA insertion into the *CYBB* locus to achieve gene correction in X-CGD patient CD34$^+$ HSPCs using AAV6 donor templates to deliver *CYBB* exon 1–13 or exon 2–13 cDNAs, both to confirm the necessity of *CYBB* intron 1 for cDNA expression from the *CYBB* promoter in corrected primary hematopoietic cells and to extend these strategies to efficient correction of patient HSPCs as a relevant cell type for clinical gene therapy. We also investigate the effect of inhibition of the NHEJ repair pathway by transient expression of an mRNA encoding i53 [38], a recently described inhibitor of the NHEJ-promoting DNA repair protein 53BP1 [39], in order to enhance the efficiency of HDR-mediated gene correction in HSPCs.

Materials and Methods

Human CD34$^+$ HSPC collection

Human CD34$^+$ HSPCs were obtained from male X-CGD patients (6 donors) or healthy donors (4 donors) after written informed consent under the auspices of National Institute of Allergy and Infectious Diseases (NIAID) Institutional Review Board-approved protocols 05-I-0213 and 94-I-0073 (ClinicalTrials.gov registration numbers NCT00001405 and NCT00128973). The conduct of these studies conforms to the Declaration of Helsinki protocols and all United States federal regulations required for protection of human subjects. Donors underwent leukapheresis after CD34$^+$ HSPC mobilization with granulocyte-colony stimulating factor (G-CSF; 15 mg/kg daily for 5 days), with all healthy donors and all but one X-CGD donor also receiving plerixafor at 12 hours before blood collection. After collection, CD34$^+$ HSPCs were purified by CliniMACS CD34$^+$ cell separation (Miltenyi Biotec; Auburn, CA) in the Cell Processing Section of the Department of Transfusion Medicine at the National Institutes of Health Clinical Center, and were cryopreserved prior to use in correction studies. X-CGD HSPCs utilized in these studies were from patients with a *CYBB* mutation downstream of exons 1 and 2 (in exon 3, exon 4, exon 7, intron 10 splice donor, or exon 12).

Mouse studies

The use of immunodeficient NOD.Cg-Prkdc^{scid} Il2rg^{tm1Wjl}/SzJ (NSG) mice (The Jackson Laboratory; Bar Harbor, ME) for xenotransplant studies was approved by the NIAID Institutional Animal Care and Use Committee under animal use protocol LCIM-1E. All mice were maintained under specific pathogen-free conditions at an American Association for the Accreditation of Laboratory Animal Care (AAALAC) accredited animal facility and housed in accordance with the procedures outlined in the Guide for the Care and Use of Laboratory Animals. The conduct of these studies conformed to AAALAC International guidelines and all U.S. federal regulations governing the protection of research animals.

CRISPR/Cas9 sgRNAs and AAV6 donor templates

Chemically modified synthetic sgRNAs targeting sites in *CYBB* exon 1 or exon 2 were commercially synthesized (Synthego; Menlo Park, CA or TriLink Biotechnologies; San Diego, CA) with 2'-O-methyl 3' phosphorothioate modifications at the first 3 and last 3 nucleotides for increased RNA stability and enhanced CRISPR/Cas9 editing activity [40]. The CRISPR target sequence at the start of *CYBB* exon 1 (corresponding to CYBB1-sg3 sgRNA for correction strategy 1) was CACAGCCCAGTTCCCCATGGTGG (with the protospacer adjacent motif or PAM sequence underlined); target sequences in exon 2 were TTGTGCAGCTGGTTTGGCTGGGG (corresponding to CYBB2-sg8 sgRNA targeting the beginning region of exon 2 for correction strategy 2) or CCCGGTAATACCAGACAAAGAGG (corresponding to CYBB2-sg3 sgRNA targeting further downstream within exon 2 for correction strategy 3).

Plasmids encoding AAV donor DNA template constructs for these correction strategies (depicted in Fig. 1) were commercially synthesized (GenScript; Piscataway, NJ or Integrated DNA Technologies; Coralville, IA) to contain a codon-optimized *CYBB* cDNA [36, 41] (1713-bp encompassing exons 1–13 for strategy 1 or 1668-bp encompassing exons 2–13 for strategies 2 and 3) and either an ~230-bp bovine growth hormone (BGH) poly-adenylation (poly-A) signal [42] (for strategies 1 and 2) or an ~530-bp rabbit beta-globin poly-A signal [43, 44] (for strategy 3). An alternative AAV donor construct for strategy 1 was designed to include a ~600-bp woodchuck hepatitis virus post-transcriptional regulatory element (WPRE) for enhanced gene expression [45, 46]; this WPRE was also included in the construct for strategy 2. The codon-optimized *CYBB* cDNAs include silent mutations to the Cas9 PAM sequence and other portions of the target sequence to prevent Cas9-mediated cutting of the donor DNA template prior to or after targeted insertion. Additionally, the cDNA expression constructs in all of the donor templates are flanked on either end by ~400-bp homology arms corresponding to sequences matching the genomic *CYBB* sequences on either side of the Cas9 cut site, and each vector contains ITRs for AAV packaging. AAV vectors were commercially packaged (Vigene Biosciences; Rockville, MD or SignaGen Laboratories; Frederick, MD) from these plasmid constructs using AAV6 capsid containing Y705F and Y731F tyrosine-to-phenylalanine capsid mutations for enhanced transduction of HSPCs [47], and AAV titers were determined by the manufacturers using qPCR detection of ITRs to quantify viral genome copies.

Targeted genome editing in CD34$^+$ HSPCs

Cryopreserved CD34$^+$ HSPCs were thawed and then pre-stimulated by culturing at a density of 0.2–0.5 × 10^6 cells per mL for 48–72 hours at 37°C and 5% CO_2 to induce proliferation of quiescent cells in HSPC medium consisting of StemSpan SFEM II serum-free medium (STEMCELL Technologies; Vancouver, Canada) containing 100 ng/mL each of human stem cell factor, Flt3-ligand, thrombopoietin, and interleukin-6 (R&D Systems, Minneapolis, MN), supplemented with 0.75 μM of StemRegenin-1 and 35 nM of UM171 (STEMCELL Technologies). For targeted genome editing experiments, CRISPR/Cas9 ribonucleoprotein (RNP) complexes were formed by adding 16.4 μg (100 pmol) of SpCas9 protein (Integrated DNA Technologies) and 250–500 pmol of chemically modified sgRNA to 100 μL of MaxCyte electroporation buffer (MaxCyte; Gaithersburg, MD) or P3 Nucleofector solution

(Lonza; Morristown, NJ), then incubating for 10–15 minutes at room temperature. In some experiments, 3.5–14 pmol of SpCas9 mRNA (made using the mMESSAGE mMACHINE T7 ULTRA kit; Thermo Fisher Scientific; Waltham, MA) was used instead of Cas9 protein in the electroporation mixture. For studies on enhancement of HDR by transient inhibition of 53BP1 during gene editing, 48–67 pmol of mRNA containing pseudouridine in place of uridine, an enzymatically added 5' cap with a cap 1 structure, and an enzymatically added poly-A tail with >175 A residues (CELLSCRIPT; Madison, WI) encoding i53 protein [38] was included in the electroporation mixture. Between 1 and 10 million HSPCs were resuspended in the electroporation mixture immediately prior to electroporation using a MaxCyte GT system with program HPSC34–3 (MaxCyte) or using a 4D-Nucleofector system with program DZ-100 (Lonza). Cells were then resuspended in HSPC medium, and AAV6 was added at a multiplicity of infection (MOI) of 5×10^3 to 1×10^5 viruses per cell immediately after electroporation. Cells were transduced for 18–48 hours in culture at 37°C, 5% CO_2 at a density up to 0.5×10^6 cells per mL, followed by media change to remove residual AAV. Cell viability was assessed at 3 days after electroporation by trypan blue exclusion stain (0.4% solution; Lonza) using a hemocytometer.

Molecular analysis of targeted editing in HSPCs

Genomic DNA was extracted (by QIAGEN DNeasy Blood & Tissue kit; QIAGEN; Germantown, MD) from HSPCs at 3–5 days post-electroporation for analysis of indels and targeted donor template insertion efficiency. Indel activity of CRISPR/Cas9 (in the absence of AAV6 transduction) was determined by ICE analysis [48] (https://ice.synthego.com) of Sanger sequencing runs from high-fidelity PCRs of *CYBB* exon 1 or exon 2 regions. Indel analysis for CYBB1-sg3 sgRNA targeting *CYBB* exon 1 for correction strategy 1 was performed using forward primer: 5'-TGTGACTGGATCATTATAGACC-3' with reverse primer: 5'-AAGCTAGAAGTGAGCCCC-3'. Indel analysis for CYBB2-sg8 sgRNA targeting *CYBB* exon 2 for strategy 2 was performed using forward primer: 5'-TGGCCTGCTATCAGCTACC-3' with reverse primer: 5'-ACTCCTGGATGGATTGCTC-3', and analysis for CYBB2-sg3 sgRNA for strategy 3 was performed using forward primer: 5'-TTTAGCTGATGAGAATTCACTAGC-3', reverse primer: 5'-TTTAAGCTAAACAATGGCACATGG-3', and sequencing primer: 5'-ATGGGGAACAACACAG-3'. The top 10 predicted off-target sites for the *CYBB* sgRNAs were determined using the COSMID web-based search tool [49] (https://crispr.bme.gatech.edu/) with parameters set to permit up to three mismatches, up to two 1-base deletions, and up to two 1-base insertions in the guide sequence followed by an NRG (either NGG or NAG) PAM sequence; PCR primers were designed for these off-target sites (Supplementary Table S1) for Sanger sequencing-based ICE analysis of off-target indel frequencies. High-fidelity PCRs for indel assays of on-target and off-target sites were performed using Q5 High-Fidelity 2x Master Mix (New England Biolabs; Ipswich, MA) or KOD One PCR Master Mix (Toyobo; Osaka, Japan).

Molecular analysis of targeted donor template insertion was performed by droplet digital PCR (ddPCR) using up to 50 ng of genomic DNA that had been digested with EcoRV restriction enzyme (Thermo Fisher Scientific) to fragment genomic DNA outside of the ddPCR target amplicon and genomic reference amplicon. Samples were analyzed using a

QX200 Droplet Digital PCR system and QuantaSoft Analysis Pro software version 1.0 (Bio-Rad; Hercules, CA) for detection of targeted donor template insertions in the *CYBB* locus in duplex reactions for detection of the *IL2RG* gene on the X-chromosome as a genomic reference, to quantify the frequency of HDR-mediated targeted insertion per genome. For strategy 1, detection of CYBB1–13 insertion was performed using forward primer: 5'-TCCAGCCTGTCAAAATCACA-3', reverse primer: 5'-TACACCCGGTAGTACCACAC-3', and hexachlorofluorescein (HEX)-labeled probe: 5'-CCTGGTGTGGCTGGGCCTGAACGT-3' (Integrated DNA Technologies), for a 515-bp amplicon. For strategy 2, detection of CYBB2–13 insertion used forward primer: 5'-AGCACCTGTGAGAACAGAAC-3', reverse primer: 5'-GGTAGTACCACACGAACAGG-3', and HEX-labeled probe: 5'-GTGCAGCTGGTTTGGCTCGGCCT-3', for a 459-bp amplicon. For strategy 3, detection of CYBB2–13 insertion used forward primer: 5'-TGTGGTAGAGGGAGGTGATTAG-3', reverse primer: 5'-AGCAGCTTCCGGGTATAGAA-3', and HEX-labeled probe: 5'-ACTTCGGTGGGATGTCATACACGC-3', for a 525-bp amplicon. *IL2RG* gene detection was performed as previously described [21] using forward primer: 5'-GGGAAGGTAAAACTGGCAAC-3', reverse primer: 5'-GGGCACATATACAGCTGTCT-3', and 6-carboxyfluorescein (FAM)-labeled probe: 5'-CCTCGCCAGTCTCAACAGGGACCCAGC-3', for a 483-bp amplicon. For each *CYBB* ddPCR assay, forward primer sequences are only present in the genome and not in the donor template, while the underlined sequences in the probes and reverse primers are unique to the codon-optimized cDNAs present in the donor template, to ensure specific detection of targeted genomic insertions.

In vitro phagocyte differentiation

Phagocyte differentiation of HSPCs was performed as previously described [50] by culturing cells for 12–16 days in Iscove's Modified Delbecco's Medium (Gibco; Thermo Fisher Scientific) supplemented with 10–20% fetal bovine serum (Atlanta Biologicals; R&D Systems; Minneapolis, MN) and 100 ng/mL human G-CSF (PeproTech), which was changed every 2–4 days, resulting in a mixed population of neutrophils and macrophages of varying maturation status (Supplementary Fig. S1a). Phagocyte morphology was assessed by Giemsa staining of cell cytospins as previously described [50, 51]; color images of stained cells were acquired using an EVOS XL Core system (Thermo Fisher Scientific), and whole image adjustments of brightness, color balance, and contrast were performed using Adobe Photoshop software (Adobe; San Jose, CA) without additional image processing. Flow cytometry analyses were performed as previously described to assess human $gp91^{phox}$ protein expression by immunostaining [50, 52] using a non-commercial unconjugated $gp91^{phox}$ (7D5) antibody [53] detected with a secondary antibody (FITC; BD Biosciences # 554001; San Jose, CA) and to assess ROS production by dihydrorhodamine-123 (DHR) assay [50, 51]. Where indicated specifically in the manuscript as flow cytometry analysis of neutrophils gated from differentiated phagocytes, analysis was performed on a gated high side-scatter population from forward-scatter versus side-scatter plots (Supplementary Fig. S1b) based on the well-established side-scatter properties of granulocytic neutrophil populations in flow cytometry; otherwise, analysis was performed on the entire viable cell population or in $gp91^{phox+}$ or DHR^{+} gated neutrophils where specified. Two weeks of

phagocyte differentiation culture was chosen as the peak time point for production of mature gp91^{phox+} neutrophils (Supplementary Fig. S1c); further culture resulted in a reduction in total cell numbers and a diminished gated neutrophil population (data not shown). Flow cytometry was performed using a FACSCalibur or FACSCanto system (BD Biosciences) with analysis conducted using FlowJo version 9.9.6 software for macOS (TreeStar Inc.; Ashland, OR). Comparisons of per-cell levels of gp91^{phox} protein expression and ROS production between corrected patient cells and healthy donor control cells were performed using mean fluorescence intensities (MFIs) of the gp91^{phox+} and DHR^{+} gated populations from flow cytometry analyses.

Transplant of human HSPCs into NSG mice

Female NSG mice at 6–10 weeks of age were treated with 20 mg/kg busulfan for myelosuppressive conditioning, administered by intraperitoneal injection approximately 24 hours before transplant of 1–2 million human HSPCs via tail vein injection. For gene correction studies, X-CGD HSPCs were pre-stimulated for 48 hours prior to electroporation and AAV6 transduction, and were transplanted 2 days later. Mice received neomycin-supplemented water post-transplant for prophylaxis. At 12 weeks post-transplant, mouse peripheral blood was collected by tail venesection, lysed with ACK lysis buffer (Quality Biological, Gaithersburg, MD) for 5–7 minutes at 37º C, then immunostained for human gp91^{phox} protein expression as described above, followed by immunostaining with antibody to human CD45 pan-leukocyte marker (APC; BD Biosciences #: 555485), for flow cytometry analysis of CD45^{+} human hematopoietic cell engraftment and gene correction in hematopoietic cells derived from engrafted human HSPCs. Mouse bone marrow and spleen were harvested at 16 weeks post-transplant, and cells were analyzed for gp91^{phox} expression (spleen) and immunostained for CD45 (PE; BD Biosciences #: 555483), CD33 myeloid (APC; BD Biosciences # 551378; APC), and CD19 B cell (PerCP-Cy5.5; BioLegend #302230; San Diego, CA) hematopoietic lineage markers (marrow and spleen) as described above. Engrafted human CD34^{+} HSPCs were isolated from bone marrow of individual mice using CD34 magnetic-activated cell sorting microbeads (Miltenyi Biotec) and were cultured separately *in vitro* for 12–16 days in phagocyte differentiation medium as described above to obtain mature human phagocytes for DHR analysis of functional correction of ROS production. For the mouse transplant study, we studied group sizes of 4 or more mice (n = 4 mice each for control groups transplanted with healthy donor HSPCs or naive X-CGD patient HSPCs and n = 6 mice for the experimental group transplanted with corrected X-CGD HSPCs) for statistical analysis of engraftment levels of assessed cell populations (CD45^{+}, CD33^{+}, CD19^{+}, gp91^{phox+}). Mice from age-matched littermates were randomly allocated into groups before injection with busulfan; no investigator blinding was performed during HSPC injection or subsequent analysis of cell populations. No transplanted mice were excluded from analysis.

Statistical analysis

Statistical analyses were performed using GraphPad Prism 8.0.1 software for macOS or 8.4.3 software for Windows (GraphPad Software, San Diego, CA). Sample sizes for each experimental group were listed in figure legends, and individual data points were plotted on all graphs along with mean ± SD; at least 3 replicates were performed for each group to

provide sufficient sample sizes for statistical comparisons (each replicate in a group comes from a separate experiment, except for samples from mouse transplants where each replicate is from an individual mouse in the same transplant experiment). Differences were tested using Mann-Whitney test (comparing 2 groups of unpaired nonparametric samples), Wilcoxon matched pairs test (comparing 2 groups of paired nonparametric samples), two-tailed unpaired Welch's t-test (comparing 2 groups with unequal variance), or one-way ANOVA with Tukey's multiple comparisons test (comparing >2 groups) where indicated. Significances were indicated as: *p<0.05, ***p<0.001, and ****p<0.0001; ns = not significant.

Results

Targeted CYBB cDNA insertion into CYBB exon 1 or exon 2

We previously reported that the targeted insertion of a full-length *CYBB* exon 1–13 cDNA plus a poly-A signal into the start site of the endogenous *CYBB* exon 1 in male X-CGD patient iPSCs failed to restore gp91^{phox} expression upon phagocyte differentiation, apparently due to the elimination of critical sequences in intron 1 necessary for expression from the *CYBB* promoter [36]. To determine whether intronic elements are likewise required for cDNA expression from the *CYBB* promoter in adult somatic HSPCs, we assessed HDR-mediated targeted insertion of a codon-optimized full-length *CYBB* exon 1–13 cDNA [41] and a BGH poly-A signal into the beginning of the endogenous *CYBB* exon 1 in male X-CGD patient HSPCs, using a CRISPR/Cas9 sgRNA (CYBB1-sg3) delivered by electroporation followed by transduction with an AAV6 donor template of the sequences to be inserted with homology arms flanking the endogenous CRISPR/Cas9 cut site (Fig. 1a), referred to here as correction strategy 1; an alternative to this AAV6 donor template containing an added WPRE for enhanced gene expression [45, 46] was also assessed (referred to as correction strategy 1 +WPRE). We also assessed two additional strategies (correction strategies 2 and 3) for targeted insertion of codon-optimized *CYBB* exon 2–13 cDNAs [36, 41] into exon 2 of the *CYBB* locus, thereby retaining the endogenous intron 1 in the resulting transcript. Correction strategy 2 utilized a CRISPR/Cas9 sgRNA (CYBB2-sg8) targeting the beginning region of the endogenous exon 2 for insertion of a codon-optimized exon 2–13 cDNA [41] together with a BGH poly-A signal [42] and a WPRE using an AAV6 donor template containing homology arms flanking the endogenous cut site (Fig. 1b). Correction strategy 3 utilized a CRISPR/Cas9 sgRNA (CYBB2-sg3) targeting further downstream within exon 2 for replacement of the entire endogenous exon 2 sequence with a codon-optimized exon 2–13 cDNA [36] and a poly-A signal derived from the rabbit beta-globin gene [43, 44], using an AAV6 donor template containing a 5' homology arm corresponding to intron 1 sequences ending at the splice acceptor site located 32 nucleotides upstream from the Cas9 cut site and a 3' homology arm corresponding to intron 2 sequences beginning at the splice donor site located 64 nucleotides downstream from the Cas9 cut site (Fig. 1c). Both BGH and rabbit beta-globin poly-A signals are strong transcriptional terminators [42–44] commonly used in gene transfer vectors, although there are conflicting reports regarding which poly-A mediates higher gene expression [54, 55], suggesting that their effects may be context dependent. The BGH poly-A signal used in strategies 1 and 2 is shorter than the rabbit beta-globin poly-A signal used in strategy 3 (~230-bp versus ~530-

bp); the shorter BGH poly-A is frequently used in AAV donor templates for HDR [17, 19, 21, 56] where small regulatory elements are desirable due to the size limitations of vector packaging. This smaller BGH poly-A was chosen for strategies 1 and 2 to more readily accommodate the additional size of a WPRE, which is frequently used in gene transfer vectors for general enhancement of gene expression [35, 45, 46], including lentiviral vectors for *CYBB* cDNA expression from exogenous promoters [7, 8, 41]. Consequently, correction strategies 1 and 2 may be regarded as employing generalized vector designs including common regulatory elements that are not specific to defined requirements for *CYBB* expression from its endogenous promoter (except for the modification from strategy 1 to strategy 2 of targeting correction at exon 2 based on our prior study in iPSCs); strategy 3 represents a more tailored approach to *CYBB* exon 2–13 correction with fewer foreign regulatory elements (consisting of *CYBB* exon 2–13 cDNA with rabbit beta-globin poly-A but lacking a WPRE), matching the exon 2–13 donor template design from our prior iPSC study that achieved physiological levels of gp91^{phox} expression in iPSC-derived phagocytes from the *CYBB* promoter without additional regulatory elements.

The cutting activity of the CYBB1-sg3 sgRNA targeting *CYBB* exon 1 for strategy 1 in male X-CGD patient or male healthy donor control HSPCs was 66% (mean) by ICE analysis of indel formation, while the CYBB2-sg8 and CYBB2-sg3 sgRNAs targeting *CYBB* exon 2 for strategies 2 and 3 exhibited cutting activities of 85% and 82% (mean), respectively (Fig. 2a and Supplementary Fig. S2); no indels were detected at the top 10 predicted off-target sites for these sgRNAs (Supplementary Fig. S3). Using un-optimized editing conditions, targeted insertion of the full-length *CYBB* exon 1–13 cDNA without the WPRE was detected by ddPCR analysis in 33% (mean) of X-CGD patient HSPCs (Fig. 2b), comparable to levels detected for strategy 1 +WPRE (mean of 46%), strategy 2 (mean of 39%), and strategy 3 (mean of 31%). However, despite the similar targeted insertion efficiencies between these strategies, there was little or no detectable gp91^{phox} protein expression above background levels for strategy 1 in neutrophil-gated phagocytes following *in vitro* differentiation of X-CGD HSPCs (Fig. 3a), consistent with our previous findings in iPSCs [36], while strategy 1 +WPRE resulted in measurable restoration of gp91^{phox} expression in a subset of the corrected neutrophil-gated phagocytes compared to healthy control cells (Fig. 3a), and targeting of exon 2 with either strategy 2 or strategy 3 resulted in substantial restoration of gp91^{phox} expression in neutrophil-gated phagocytes (Fig. 3b, c).

Based on comparisons of per-cell levels of gp91^{phox} expression from the MFIs of gp91^{phox+} gated neutrophils by flow cytometry immunostaining relative to levels in healthy donor controls, correction of X-CGD HSPCs using strategy 1 +WPRE only partially restored phagocyte expression of gp91^{phox} expression, resulting in mean per-cell expression levels that were 41% of levels measured in healthy controls (Fig. 3d, e). In contrast, correction with strategy 2 resulted in mean per-cell levels of gp91^{phox} expression that were 78% of levels in gp91^{phox+} healthy donor controls, and strategy 3 resulted in expression levels that were 98% of those in healthy controls (Fig. 3d, e), demonstrating full phenotypic correction of the gp91^{phox} expression defect of X-CGD by the exon 2 targeted correction strategies. Together this indicates that inclusion of a WPRE could only partially compensate for the absence of intron 1 to express exon 1–13 cDNA from the *CYBB* promoter, while the targeted insertion of exon 2–13 cDNA with a strong poly-A signal [43, 44] was sufficient for achieving

physiologically normal levels of gp91^{phox} protein expression when intron 1 was retained, without requiring a WPRE or other exogenous regulatory elements. Similar results were observed for functional correction of ROS production measured by DHR assay in differentiated neutrophil-gated phagocytes, demonstrating that strategy 1 +WPRE resulted in only partial restoration of ROS production to mean per-cell levels 47% of those measured in healthy donor controls (Fig. 4a, c), while correction with strategies 2 and 3 both resulted in full restoration of ROS production to mean per-cell levels that were 92% and 94%, respectively, of healthy controls (Fig. 4b, c) based on the MFIs of DHR^{+} gated neutrophils.

Increased targeted insertion of AAV6 donor template in HSPCs by 53BP1 inhibition

For X-CGD, healthy or gene corrected phagocytes do not possess a survival or proliferative advantage over diseased ones, therefore a high frequency of genome editing is necessary in order to achieve a clinically beneficial threshold of functional correction [8, 57]. In order to optimize HDR-mediated targeted insertion efficiencies of exon 2–13 cDNA constructs in X-CGD HSPCs, we investigated the effects of transient inhibition of 53BP1 in the NHEJ pathway using i53 mRNA [38]. Enhancement of HDR by i53 expression for increased targeted insertion had previously been reported in immortalized human cell lines [38, 58–60], but not in primary human cells. HSPCs from healthy male donors were used for our initial targeted insertion optimization studies, in order to model the mono-allelic *CYBB* target of male X-CGD patients. Inclusion of i53 mRNA with CRISPR/Cas9 RNP (CYBB2-sg3) complexes during HSPC electroporation did not alter the overall frequency of indel formation at the *CYBB* target site in the absence of AAV6 donor template (Fig. 5a). However, when combined with AAV6 transduction (using donor template for strategy 3) at a MOI of 1×10^5 viruses per cell, i53 resulted in approximately 1.5-fold increase in targeted insertion in HSPCs (Fig. 5b) based on ddPCR analysis (mean targeted insertion frequencies of 31.0% without i53 versus 46.7% with i53). Transient expression of i53 had no significant effect on the viability of transfected HSPCs either in the presence or absence of AAV6 transduction (Fig. 5c), however AAV6 itself significantly reduced HSPC viability. When applied to X-CGD patient HSPCs, the enhancement of targeted insertion efficiency by i53 likewise resulted in a 1.5-fold increase in phenotypic correction based on the percentage of phagocytes expressing gp91^{phox} (mean of 20.2% without i53 versus 30.3% with i53) following differentiation from corrected X-CGD patient HSPCs (Fig. 5d, e).

In vivo engraftment of gene corrected HSPCs

In order to assess engraftment potential following gene correction, X-CGD patient HSPCs were corrected by *CYBB* exon 2–13 cDNA insertion using strategy 2 under optimized targeted insertion conditions with i53 mRNA and an AAV6 MOI of approximately 1×10^5, and were then transplanted into busulfan-preconditioned immunodeficient NSG mice (n = 6 transplanted mice for corrected X-CGD HSPC transplants; n = 4 transplanted mice each for healthy control HSPC and X-CGD naive HSPC transplants). The pre-transplant HSPC population exhibited 60% targeted correction by ddPCR analysis (526 copies of CYBB2–13 targeted insertion detected per 880 genomic reference copies per 20 μL ddPCR reaction), and 48% of neutrophil-gated phagocytes expressed gp91^{phox} upon *in vitro* phagocyte differentiation (Fig. 6a). The mean human cell engraftment detected in peripheral blood at 12 weeks post-transplant was 15.9% for the exon 2–13 cDNA corrected cells based on

human CD45 immunostaining, similar to transplanted naive X-CGD (mean of 22.9%) or healthy donor (mean of 16.8%) control HSPCs (Fig. 6b, **c**). A subset of the engrafted corrected X-CGD cells exhibited restored gp91^{phox} expression *in vivo* (Fig. 6b, d), although at lower contribution than in the input HSPC population used for transplant (mean value of 7.6% of engrafted human CD45^{+} cells were gp91^{phox+} in Fig. 6d versus 48% gp91^{phox+} for *in vitro* differentiated phagocytes in Fig. 6a), while healthy donor control cells exhibited similar gp91^{phox+} population percentages post-transplant as in the pre-transplant population (Fig. 6d versus Fig. 6a). Mouse bone marrow was harvested at 16 weeks post-transplant for analysis of human CD45^{+} hematopoietic, CD19^{+} B cell and CD33^{+} myeloid cell lineages (Supplementary Fig. S4), which confirmed the presence of multilineage human hematopoietic cell engraftment in all mice transplanted with corrected X-CGD CD34^{+} HSPCs. Mouse spleen was also harvested for analysis of gp91^{phox} expression in human CD45^{+} hematopoietic cells (Supplementary Fig. S5); the gp91^{phox+} gated cell populations in spleen (mean of 5.3% gp91^{phox+} cells in CD45^{+} gated populations in X-CGD corrected HSPC transplants) contained both CD33^{+} myeloid and CD19^{+} B cell lineages, similar to healthy donor HSPC transplant control, indicating multilineage engraftment of corrected cells. In order to obtain a robust population of mature human phagocytes from engrafted HSPCs for functional analysis, human CD34^{+} cells were sorted from the bone marrow of individual mice and then differentiated for 2 weeks *in vitro* with human G-CSF to produce mature human phagocytes for assessment of ROS production. The neutrophil-gated phagocytes differentiated from corrected X-CGD engrafted CD34^{+} HSPCs exhibited functional restoration of ROS production (Fig. 6e; mean of 4.5% DHR^{+} cells) at mean per-cell levels that were 93% of levels in healthy control neutrophils (Fig. 6f), confirming that a population of gene corrected CD34^{+} HSPCs was maintained *in vivo* following engraftment, albeit with decreased percentages of functionally corrected cells than the level of targeted gene insertion initially detected in the pre-transplant HSPC population, consistent with the gp91^{phox} expression data in peripheral blood and spleen.

Discussion

Here we demonstrate several strategies for HDR-mediated targeted insertion of *CYBB* cDNAs from AAV6-based donor DNA templates into the single *CYBB* locus in male X-CGD patient HSPCs using CRISPR/Cas9, in order to achieve regulated expression of the inserted cDNA by the endogenous *CYBB* promoter for functional correction of patient cells. Targeted insertion of an intronless full-length *CYBB* exon 1–13 cDNA and a poly-A signal into the start site of exon 1 of the *CYBB* locus could be achieved efficiently but resulted in little or no detectable expression of gp91^{phox} protein upon phagocyte differentiation, possibly due to the elimination of one or more important transcriptional regulatory elements in *CYBB* intron 1, such as a putative NF-κB enhancer element that normally interacts with a distant upstream NF-κB binding site and with the *CYBB* promoter to regulate *CYBB* expression in phagocytes [61]. The lack of detectable gp91^{phox} expression after targeted insertion of exon 1–13 cDNA is consistent with our previous findings in X-CGD patient iPSCs [36], validating the use of iPSCs for modeling the efficacy of targeted insertion strategies for functional correction and expression in relevant cell lineages. Inclusion of a WPRE with the exon 1–13 cDNA partially restored gp91^{phox} expression in the present study,

but was unable to completely compensate for the loss of intron 1. A similar gene editing strategy targeting the exon 1 start site of the *CD40LG* gene for full-length cDNA insertion in T cells of patients with X-linked hyper-IgM syndrome was shown by Hubbard *et al.* [35] to fully restore normal physiological levels of CD40L protein expression and its functional activity; additionally, insertion of an intronless full-length *CYBB* exon 1–13 cDNA under the control of an exogenous promoter using safe-harbor targeted insertion [13] or using retroviral or lentiviral vectors [3, 4, 7, 8, 62] in X-CGD patient HSPCs has previously been shown to result in substantial $gp91^{phox}$ expression in phagocytes, in contrast to our present data regarding intronless full-length cDNA expression from the *CYBB* promoter. These findings reflect the disparity in the regulation of expression between different genes and promoters, and highlight the importance of designing gene editing strategies tailored for the specific locus and disease.

As an alternative approach for correction of *CYBB* mutations occurring downstream of intron 1 (encompassing ~90% of reported X-CGD patients) [1], we also tested the targeted insertion of either of two *CYBB* exon 2–13 cDNA constructs (differing in the presence or absence of a WPRE as an exogenous regulatory element for enhanced expression) and a poly-A signal into exon 2 of the *CYBB* locus, to retain the endogenous *CYBB* intron 1 in the resulting transcript. Efficient targeted correction of X-CGD patient HSPCs could be achieved with either exon 2–13 cDNA construct, restoring $gp91^{phox}$ protein expression and ROS production in phagocytes derived from gene corrected HSPCs of X-CGD patients to normal or near-normal physiological levels, exceeding the per-cell levels previously reported for *CYBB* cDNA transfer into X-CGD HSPCs by safe-harbor targeted insertion [20] or by lentiviral vector insertion except at high vector copy numbers [7, 8, 62]. These data indicate that retention of *CYBB* intron 1 is sufficient to mediate physiologically normal levels of $gp91^{phox}$ expression from the *CYBB* promoter, without requiring the inclusion of additional exogenous regulatory elements (such as a WPRE) in the inserted donor template, other than a strong poly-A signal such as rabbit beta-globin poly-A [43, 44]. These findings highlight again the utility of tailoring the design of targeting strategies and donor template constructs to include the appropriate regulatory elements necessary for optimal expression of the target gene.

Of the remaining ~10% of X-CGD patients that are not treatable by an exon 2–13 correction strategy, approximately 4% have mutations in the upstream region including exon 1, the intron 1 splice donor site, or the *CYBB* promoter [1], which would require the development of alternative strategies for targeted correction of the *CYBB* locus to those described here, such as the targeted insertion of a donor template encompassing only the upstream region for correction of this subset of patients. Another strategy would be the incorporation of *CYBB* intron 1 in a complete donor template with exon 1–13 cDNA for simultaneous correction of all *CYBB* mutations. However, the ~2-kb size of *CYBB* intron 1 and the packaging size limits of AAV would complicate its inclusion in a single AAV6 donor template containing the necessary *CYBB* exon 1–13 cDNA, poly-A signal, and homologous sequences, particularly given the difficulties for achieving the desired targeted homologous recombination that would be posed by the inclusion of the additional 2-kb of homologous intron 1 sequences interrupting the codon-optimized exon 1 and exon 2–13 cDNA sequences to be inserted; however, this approach might be enabled by the identification and inclusion

of only the minimal critical sequences within *CYBB* intron 1 needed for achieving physiologically normal levels of expression, or alternatively by the inclusion of exogenous enhancer elements in place of *CYBB* intron 1 that are suitably strong and cell lineage-appropriate. The remaining ~6% of X-CGD patients have large deletions of the X-chromosome encompassing *CYBB* promoter and exon regions and in some cases neighboring genes [1], which would preclude targeted repair by any of these strategies, necessitating other HSPC gene therapy approaches such as *CYBB* cDNA transfer using a lentiviral vector containing a chimeric promoter for myeloid-specific $gp91^{phox}$ expression [7, 8] or targeted insertion into the safe-harbor AAVS1 locus [13] as we previously described, possibly with additional vector enhancements to achieve normal physiological levels of expression and functional correction per cell.

A number of studies have assessed chemical or molecular modulation of DNA repair pathway components to enhance HDR-mediated genome editing in human cells, including enhancement of the activity of HDR pathway components Rad51 [58, 63] and CtIP [64–66], or inhibition of NHEJ pathway components DNA ligase IV [63, 65, 67–69], Ku70/Ku80 [65, 69], DNA-PK [70–72], and 53BP1 [38, 56, 58–60, 73]. However, most of these studies have been conducted in immortalized cell lines or pluripotent stem cells rather than primary cells, and effects appear to be cell type-dependent. Thus far, the majority of agents tested in $CD34^+$ HSPCs appear ineffective at enhancing HDR in these cells, with only a few resulting in substantial increases in targeted insertion of donor templates [71, 72]. Riesenberg and Maricic [71] reported that NU7026, a chemical inhibitor of DNA-PK, enhanced CRISPR/Cpf1-mediated HDR of an ssODN donor template in $CD34^+$ HSPCs by 1.7-fold, but this treatment reduced cell viability to ~80% relative to edited controls; HDR enhancement by NU7026 was increased to 2.6-fold when combined with Trichostatin A and NSC 15520 to increase activities of ATM kinase and Replication Protein A in the HDR pathway, but this also further reduced HSPC viability to 65%. Likewise, Jayavaradhan *et al.* [72] showed that NU7441, another inhibitor of DNA-PK, enhanced HDR of an AAV6 donor template in $CD34^+$ HSPCs by 2-fold, but reduced cell viability to ~65% compared to controls corrected with only CRISPR/Cas9 and AAV6. Additionally, Lomova *et al.* [66] reported ~4-fold enhancement of the HDR/NHEJ ratio for AAV6 donor template in HSPCs using geminin-modified Cas9 for reduced nuclease activity during G1 phase when cells were pre-treated with a CDK1 inhibitor to transiently arrest cell cycle progression at S/G2 phases; however, this approach predominantly decreased the incidence of NHEJ-induced indels rather than substantially increasing HDR, and cell viability was decreased ~50% by the CDK1 inhibitor.

In the current study, we assessed inhibition of 53BP1, an early key regulator of DSB repair pathway choice that promotes NHEJ over HDR [39]. Canny *et al.* [38] recently demonstrated that transient expression of i53, an engineered inhibitor of 53BP1, enhances the efficiency of HDR-mediated targeted insertion of ssODNs or double-strand plasmid DNA donor templates in immortalized human cell lines; similar results were reported at various gene loci in immortalized human cells in subsequent studies [58–60]. However, the effects of i53 expression on enhancing HDR was not reported in primary human cells or for insertion of AAV-based donor DNA templates. In our study, co-transfection of Cas9 RNP with i53 mRNA at the concentrations tested was well-tolerated in primary $CD34^+$ HSPCs and resulted in ~1.5-fold increased targeted insertion of AAV6 donor template without

further reducing cell viability compared to correction with Cas9 RNP and AAV6 alone, demonstrating efficacy of 53BP1 inhibition for enhancing HDR in this clinically relevant cell type for AAV donor-based targeted insertion therapies; however, these effects were primarily observed in HSPCs capable of *in vitro* differentiation into phagocytes, requiring further assessment of long-term effects in engrafting HSPCs. A recent study by Jayavaradhan *et al.* [56] tested a similar approach of inhibiting 53BP1 activity to enhance HDR in immortalized human cell lines, by fusing Cas9 to a dominant-negative mutant of 53BP1 to localize its effects on NHEJ to Cas9 target sites; given the efficacy of 53BP1 inhibition in HSPCs in our study, this Cas9 fusion might provide a further safety improvement for enhancing HDR-mediated genome editing in HSPCs, by limiting potential undesired effects of transient genome-wide NHEJ inhibition.

Our described strategies for *CYBB* exon 2–13 correction of X-CGD patient $CD34^+$ HSPCs resulted in at least a partial retention of engraftment potential, as functional restoration of ROS production could be detected in phagocytes derived from HSPCs engrafted in NSG mice. However, while the overall level of human $CD45^+$ cell engraftment in NSG mice was similar between the treated HSPCs and the naive X-CGD patient or healthy donor controls, the subset of successfully gene-corrected cells present within those engrafted human cells at 12 to 16 weeks post-transplant was markedly lower than was present in the treated $CD34^+$ HSPC population that was initially transplanted, demonstrating a ~84–89% decrease from the initial population based on $gp91^{phox}$ expression (from 48% initially in pre-transplant neutrophils to ~7.6% in week 12 blood and ~5.3% in week 16 spleen) with 4.5% DHR^+ neutrophils derived from sorted $CD34^+$ cells from mouse bone marrow, reducing the percentage of corrected cells below the predicted threshold of 10% functionally normal neutrophils that would provide lasting clinical benefit to X-CGD patients [8] based on studies of female carriers of X-CGD [57]. Similar substantial reductions in editing efficiencies have been reported in most studies to date that have assessed transplantation of human HSPCs after HDR-mediated editing using AAV6 donor templates. Dever *et al.* [19] reported ~78% reduction in marking following CRISPR/Cas9-mediated insertion of GFP cDNA into the *HBB* locus in healthy donor HSPCs without additional selection for gene-edited cells (from 16% GFP^+ pre-transplant to 3.5% GFP^+ human cells in mouse bone marrow at 16 weeks post-transplant). In our prior study for AAVS1 safe harbor targeted gene insertion [20] we reported ~75% reduction in targeted insertion post-engraftment for X-CGD HSPCs targeted with ZFNs to *CYBB* cDNA at the AAVS1 locus (from 15% $gp91^{phox+}$ pre-transplant to 3.7% $gp91^{phox+}$ human cells in mouse bone marrow at 8 weeks post-transplant), and ~81% reduction in marking for targeted insertion of Venus fluorescence gene in healthy donor cells (from 57% $Venus^+$ pre-transplant to 10.8% $Venus^+$ in mouse bone marrow). Pattabhi *et al.* [22] reported ~97% reduction in gene-targeted cells using CRISPR/Cas9 with AAV6 to target the *HBB* locus in healthy donor HSPCs to induce the sickle cell mutation (from 24.3% HDR-targeted pre-transplant to 0.7% HDR-targeted human cells in mouse bone marrow at 12–14 weeks post-transplant). Romero *et al.* [23] similarly reported ~90% reduction in CRISPR/Cas9-mediated HDR editing of the *HBB* locus to induce the sickle mutation in healthy donor HSPCs (from 46.2% HDR-targeted pre-transplant to 4.8% HDR-targeted human cells in mouse bone marrow at 4 months post-transplant) and ~85% reduction in ZFN-mediated HDR editing (from 32.6% pre-transplant

to 5% in human cells in mouse bone marrow at 4 months post-transplant). Schiroli *et al.* [24] reported ~88% reduction in marking using AAV6 to target insertion of a GFP cDNA into the AAVS1 or *IL2RG* locus in cord blood HSPCs (from ~59% HDR-targeted pre-transplant to ~7% GFP^+ human cells in mouse bone marrow at >20 weeks post-transplant). Schiroli *et al.* further identified that CRISPR/Cas9 and AAV6 delivery in HSPCs each induced p53-mediated activation of a DNA damage response pathway which impaired HSPC engraftment and long-term repopulation capacity; this is consistent with the significantly reduced HSPC viability that we observed following AAV6 transduction in combination with CRISPR/Cas9 electroporation in our study. Schiroli *et al.* also reported that the functional impairment of HSPC proliferation and engraftment caused by DNA damage response to CRISPR/Cas9 and AAV6 could be overcome by transient inhibition of p53 using GSE56 mRNA (encoding a dominant negative truncated form of p53) during genome editing of HSPCs, thereby enabling greater retention of HSPC engraftment and repopulation capacity in corrected cells [24]. These prior studies involving AAV6-mediated HDR in healthy donor HSPCs at other gene loci strongly suggest that the substantial reduction in X-CGD corrected cells post-engraftment that we report here is not the result of a particular susceptibility of X-CGD patient HSPCs to the damaging effects of CRISPR/Cas9 or AAV6 transduction, particular effects of targeting the *CYBB* locus, or some other unique aspect of our correction methodology, although we cannot discount the possibility that i53 may have affected engraftment based on the studies performed here. Interestingly, it has been reported that 53BP1 stimulates p53-dependent transcriptional responses to DNA damage independently of 53BP1's role in the choice of DSB repair pathways [74], which suggests that 53BP1 inhibition might have additional effects on p53-mediated DNA damage response pathways induced by CRISPR/Cas9 and AAV6 transduction; however, it is apparent from our present data that any such modulation of p53-induced DNA damage response by transient inhibition of 53BP1 using i53 did not sufficiently counteract the detrimental effects of AAV6 transduction and CRISPR/Cas9 for retention of corrected HSPCs at clinically-beneficial levels following engraftment in our current study. Additional studies assessing i53 combined with direct inhibition of p53 (by GSE56 or other agents) are needed to determine whether the enhanced HDR efficiency mediated by i53 can synergize with the protective effects of p53 inhibition on HSPC engraftment, to provide a greater improvement to HDR-mediated genome editing using AAV6 donor templates in transplantable HSPCs that may ultimately be necessary to attain clinically-beneficial levels of stable correction for X-CGD and other diseases where correction does not confer a proliferative or survival advantage to engrafted cells.

Supplementary Material

Refer to Web version on PubMed Central for supplementary material.

Acknowledgements:

We thank the patients and healthy donors for their contribution to this study, the Department of Transfusion Medicine at the National Institutes of Health Clinical Center for their collection and processing of $CD34^+$ HSPCs, and the CCR Genomics Core of the National Cancer Institute for their assistance in DNA sequencing and ddPCR analyses.

Funding: This research was supported by the Intramural Research Program of the National Institute of Allergy and Infectious Diseases, National Institutes of Health (NIH) under intramural project numbers Z01-Al-00644 and Z01-Al-00988, as well as funding to M.H.P. under NIH research grant R01-AI097320 and philanthropic gift funds from the Amon G. Carter Foundation.

References

1. Roos D, Kuhns DB, Maddalena A, Roesler J, Lopez JA, Ariga T et al. Hematologically important mutations: X-linked chronic granulomatous disease (third update). Blood Cells Mol Dis. 2010;45(3):246–265. [PubMed: 20729109]
2. Marciano BE, Spalding C, Fitzgerald A, Mann D, Brown T, Osgood S et al. Common severe infections in chronic granulomatous disease. Clin Infect Dis. 2015;60(8):1176–1183. [PubMed: 25537876]
3. Stein S, Ott MG, Schultze-Strasser S, Jauch A, Burwinkel B, Kinner A et al. Genomic instability and myelodysplasia with monosomy 7 consequent to EVI1 activation after gene therapy for chronic granulomatous disease. Nat Med. 2010;16(2):198–204. [PubMed: 20098431]
4. Ulrich S, Anna P, Heidi H-G, Elena K, Ulrike K, Eleonore DR et al. Successful combination of sequential gene therapy and rescue allo-HSCT in two children with X-CGD - importance of timing. Curr Gene Ther. 2015;15(4):416–427. [PubMed: 25981636]
5. Grez M, Reichenbach J, Schwäble J, Seger R, Dinauer MC, Thrasher AJ. Gene therapy of chronic granulomatous disease: the engraftment dilemma. Mol Ther. 2011;19(1):28–35. [PubMed: 21045810]
6. Yahata T, Takanashi T, Muguruma Y, Ibrahim AA, Matsuzawa H, Uno T et al. Accumulation of oxidative DNA damage restricts the self-renewal capacity of human hematopoietic stem cells. Blood. 2011;118(11):2941–2950. [PubMed: 21734240]
7. Santilli G, Almarza E, Brendel C, Choi U, Beilin C, Blundell MP et al. Biochemical correction of X-CGD by a novel chimeric promoter regulating high levels of transgene expression in myeloid cells. Mol Ther. 2011;19(1):122–132. [PubMed: 20978475]
8. Kohn DB, Booth C, Kang EM, Pai S-Y, Shaw KL, Santilli G et al. Lentiviral gene therapy for X-linked chronic granulomatous disease. Nat Med. 2020;26(2):200–206. [PubMed: 31988463]
9. Jinek M, Chylinski K, Fonfara I, Hauer M, Doudna JA, Charpentier E. A programmable dual-RNA–guided DNA endonuclease in adaptive bacterial immunity. Science. 2012;337(6096):816–821. [PubMed: 22745249]
10. Cong L, Ran FA, Cox D, Lin S, Barretto R, Habib N et al. Multiplex genome engineering using CRISPR/Cas systems. Science. 2013;339(6121):819–823. [PubMed: 23287718]
11. Mali P, Yang L, Esvelt KM, Aach J, Guell M, DiCarlo JE et al. RNA-guided human genome engineering via Cas9. Science. 2013;339(6121):823–826. [PubMed: 23287722]
12. Moehle EA, Rock JM, Lee Y-L, Jouvenot Y, DeKelver RC, Gregory PD et al. Targeted gene addition into a specified location in the human genome using designed zinc finger nucleases. Proc Natl Acad Sci U S A. 2007;104(9):3055–3060. [PubMed: 17360608]
13. DeKelver RC, Choi VM, Moehle EA, Paschon DE, Hockemeyer D, Meijsing SH et al. Functional genomics, proteomics, and regulatory DNA analysis in isogenic settings using zinc finger nuclease-driven transgenesis into a safe harbor locus in the human genome. Genome Res. 2010;20(8):1133–1142. [PubMed: 20508142]
14. Miller JC, Tan S, Qiao G, Barlow KA, Wang J, Xia DF et al. A TALE nuclease architecture for efficient genome editing. Nat Biotechnol. 2011;29(2):143–148. [PubMed: 21179091]
15. Levetzow GV, Spanholtz J, Beckmann J, Fischer J, Kögler G, Wernet P et al. Nucleofection, an efficient nonviral method to transfer genes into human hematopoietic stem and progenitor cells. Stem Cells Dev. 2006;15(2):278–285. [PubMed: 16646674]
16. Lesueur LL, Mir LM, André FM. Overcoming the specific toxicity of large plasmids electrotransfer in primary cells in vitro. Mol Ther Nucleic Acids. 2016;5(3):e291–e291. [PubMed: 27111417]
17. Sather BD, Romano Ibarra GS, Sommer K, Curinga G, Hale M, Khan IF et al. Efficient modification of CCR5 in primary human hematopoietic cells using a megaTAL nuclease and AAV donor template. Sci Transl Med. 2015;7(307):307ra156.

18. Wang J, Exline CM, DeClercq JJ, Llewellyn GN, Hayward SB, Li PW-L et al. Homology-driven genome editing in hematopoietic stem and progenitor cells using ZFN mRNA and AAV6 donors. Nat Biotechnol. 2015;33(12):1256–1263. [PubMed: 26551060]
19. Dever DP, Bak RO, Reinisch A, Camarena J, Washington G, Nicolas CE et al. CRISPR/Cas9 β-globin gene targeting in human haematopoietic stem cells. Nature. 2016;539:384–389. [PubMed: 27820943]
20. De Ravin SS, Reik A, Liu P-Q, Li L, Wu X, Su L et al. Targeted gene addition in human $CD34^+$ hematopoietic cells for correction of X-linked chronic granulomatous disease. Nat Biotechnol. 2016;34:424–429. [PubMed: 26950749]
21. Pavel-Dinu M, Wiebking V, Dejene BT, Srifa W, Mantri S, Nicolas CE et al. Gene correction for SCID-X1 in long-term hematopoietic stem cells. Nat Commun. 2019;10(1):1634. [PubMed: 30967552]
22. Pattabhi S, Lotti SN, Berger MP, Singh S, Lux CT, Jacoby K et al. In vivo outcome of homology-directed repair at the HBB gene in HSC using alternative donor template delivery methods. Mol Ther Nucleic Acids. 2019;17:277–288. [PubMed: 31279229]
23. Romero Z, Lomova A, Said S, Miggelbrink A, Kuo CY, Campo-Fernandez B et al. Editing the sickle cell disease mutation in human hematopoietic stem cells: comparison of endonucleases and homologous donor templates. Mol Ther. 2019;27(8):1389–1406. [PubMed: 31178391]
24. Schiroli G, Conti A, Ferrari S, della Volpe L, Jacob A, Albano L et al. Precise gene editing preserves hematopoietic stem cell function following transient p53-mediated DNA damage response. Cell Stem Cell. 2019;24(4):551–565.e8.
25. Gundry Michael C, Brunetti L, Lin A, Mayle Allison E, Kitano A, Wagner D et al. Highly efficient genome editing of murine and human hematopoietic progenitor cells by CRISPR/Cas9. Cell Reports. 2016;17(5):1453–1461. [PubMed: 27783956]
26. DeWitt MA, Magis W, Bray NL, Wang T, Berman JR, Urbinati F et al. Selection-free genome editing of the sickle mutation in human adult hematopoietic stem/progenitor cells. Sci Transl Med. 2016;8(360):360ra134.
27. De Ravin SS, Li L, Wu X, Choi U, Allen C, Koontz S et al. CRISPR-Cas9 gene repair of hematopoietic stem cells from patients with X-linked chronic granulomatous disease. Sci Transl Med. 2017;9(372):eaah3480.
28. Antony JS, Latifi N, Haque AKMA, Lamsfus-Calle A, Daniel-Moreno A, Graeter S et al. Gene correction of HBB mutations in CD34+ hematopoietic stem cells using Cas9 mRNA and ssODN donors. Mol Cell Pediatr. 2018;5(1):9. [PubMed: 30430274]
29. Park SH, Lee CM, Dever DP, Davis TH, Camarena J, Srifa W et al. Highly efficient editing of the β-globin gene in patient-derived hematopoietic stem and progenitor cells to treat sickle cell disease. Nucleic Acids Res. 2019;47(15):7955–7972. [PubMed: 31147717]
30. Hoban MD, Cost GJ, Mendel MC, Romero Z, Kaufman ML, Joglekar AV et al. Correction of the sickle cell disease mutation in human hematopoietic stem/progenitor cells. Blood. 2015;125(17):2597–604. [PubMed: 25733580]
31. Pannunzio NR, Watanabe G, Lieber MR. Nonhomologous DNA end-joining for repair of DNA double-strand breaks. J Biol Chem. 2018;293(27):10512–10523. [PubMed: 29247009]
32. Miyaoka Y, Berman JR, Cooper SB, Mayerl SJ, Chan AH, Zhang B et al. Systematic quantification of HDR and NHEJ reveals effects of locus, nuclease, and cell type on genome-editing. Sci Rep. 2016;6:23549. [PubMed: 27030102]
33. Branzei D, Foiani M. Regulation of DNA repair throughout the cell cycle. Nat Rev Mol Cell Biol. 2008;9(4):297–308. [PubMed: 18285803]
34. Genovese P, Schiroli G, Escobar G, Tomaso TD, Firrito C, Calabria A et al. Targeted genome editing in human repopulating haematopoietic stem cells. Nature. 2014;510(7504):235–240. [PubMed: 24870228]
35. Hubbard N, Hagin D, Sommer K, Song Y, Khan I, Clough C et al. Targeted gene editing restores regulated CD40L function in X-linked hyper-IgM syndrome. Blood. 2016;127(21):2513–2522. [PubMed: 26903548]

36. Sweeney CL, Zou J, Choi U, Merling RK, Liu A, Bodansky A et al. Targeted repair of CYBB in X-CGD iPSCs requires retention of intronic sequences for expression and functional correction. Mol Ther. 2017;25(2):321–330. [PubMed: 28153086]
37. Shaul O. How introns enhance gene expression. Int J Biochem Cell Biol. 2017;91:145–155. [PubMed: 28673892]
38. Canny MD, Moatti N, Wan LCK, Fradet-Turcotte A, Krasner D, Mateos-Gomez PA et al. Inhibition of 53BP1 favors homology-dependent DNA repair and increases CRISPR–Cas9 genome-editing efficiency. Nat Biotechnol. 2017;36:95. [PubMed: 29176614]
39. Escribano-Díaz C, Orthwein A, Fradet-Turcotte A, Xing M, Young Jordan TF, Tkáč J et al. A cell cycle-dependent regulatory circuit composed of 53BP1-RIF1 and BRCA1-CtIP controls DNA repair pathway choice. Mol Cell. 2013;49(5):872–883. [PubMed: 23333306]
40. Hendel A, Bak RO, Clark JT, Kennedy AB, Ryan DE, Roy S et al. Chemically modified guide RNAs enhance CRISPR-Cas genome editing in human primary cells. Nat Biotechnol. 2015;33:985. [PubMed: 26121415]
41. Moreno-Carranza B, Gentsch M, Stein S, Schambach A, Santilli G, Rudolf E et al. Transgene optimization significantly improves SIN vector titers, gp91^{phox} expression and reconstitution of superoxide production in X-CGD cells. Gene Ther. 2009;16(1):111–118. [PubMed: 18784749]
42. Goodwin EC, Rottman FM. The 3'-flanking sequence of the bovine growth hormone gene contains novel elements required for efficient and accurate polyadenylation. J Biol Chem. 1992;267(23):16330–16334. [PubMed: 1644817]
43. Gil A, Proudfoot NJ. Position-dependent sequence elements downstream of AAUAAA are required for efficient rabbit β-globin mRNA 3′ end formation. Cell. 1987;49(3):399–406. [PubMed: 3568131]
44. Lanoix J, Acheson NH. A rabbit beta-globin polyadenylation signal directs efficient termination of transcription of polyomavirus DNA. EMBO J. 1988;7(8):2515–2522. [PubMed: 2847921]
45. Loeb JE, Cordier WS, Harris ME, Weitzman MD, Hope TJ. Enhanced expression of transgenes from adeno-associated virus vectors with the woodchuck hepatitis virus posttranscriptional regulatory element: implications for gene therapy. Hum Gene Ther. 1999;10(14):2295–2305. [PubMed: 10515449]
46. Zufferey R, Donello JE, Trono D, Hope TJ. Woodchuck hepatitis virus posttranscriptional regulatory element enhances expression of transgenes delivered by retroviral vectors. J Virol. 1999;73(4):2886–2892. [PubMed: 10074136]
47. Song L, Li X, Jayandharan GR, Wang Y, Aslanidi GV, Ling C et al. High-efficiency transduction of primary human hematopoietic stem cells and erythroid lineage-restricted expression by optimized AAV6 serotype vectors in vitro and in a murine xenograft model in vivo. PLoS One. 2013;8(3):e58757.
48. Hsiau T, Conant D, Rossi N, Maures T, Waite K, Yang J et al. Inference of CRISPR edits from Sanger trace data. bioRxiv. 2019:251082.
49. Cradick TJ, Qiu P, Lee CM, Fine EJ, Bao G. COSMID: A Web-based Tool for Identifying and Validating CRISPR/Cas Off-target Sites. Molecular Therapy - Nucleic Acids. 2014;3:e214.
50. Sweeney CL, Merling RK, De Ravin SS, Choi U, Malech HL. Gene editing in chronic granulomatous disease. In: Knaus UG, Leto TL (eds). NADPH Oxidases: Methods and Protocols. (Springer New York, New York, NY, 2019) pp 623–665.
51. Zou J, Sweeney CL, Chou BK, Choi U, Pan J, Wang H et al. Oxidase-deficient neutrophils from X-linked chronic granulomatous disease iPS cells: functional correction by zinc finger nuclease-mediated safe harbor targeting. Blood. 2011;117(21):5561–72. [PubMed: 21411759]
52. Merling RK, Sweeney CL, Chu J, Bodansky A, Choi U, Priel DL et al. An AAVS1-targeted minigene platform for correction of iPSCs from all five types of chronic granulomatous disease. Mol Ther. 2015;23(1):147–157. [PubMed: 25288370]
53. Yamauchi A, Yu L, Pötgens Andy JG, Kuribayashi F, Nunoi H, Kanegasaki S et al. Location of the epitope for 7D5, a monoclonal antibody raised against human flavocytochrome b_{558}, to the extracellular peptide portion of primate gp91^{phox}. Microbiol Immunol. 2013;45(3):249–257.

54. Komiya E, Kondoh M, Mizuguchi H, Fujii M, Utoguchi N, Nakanishi T et al. Characteristics of transcription-regulatory elements for gene expression from plasmid vectors in human trophoblast cell lines. Placenta. 2006;27(9):934–938. [PubMed: 16600369]
55. Yew NS, Wysokenski DM, Wang KX, Ziegler RJ, Marshall J, McNeilly D et al. Optimization of plasmid vectors for high-level expression in lung epithelial cells. Hum Gene Ther. 1997;8(5):575–584. [PubMed: 9095409]
56. Jayavaradhan R, Pillis DM, Goodman M, Zhang F, Zhang Y, Andreassen PR et al. CRISPR-Cas9 fusion to dominant-negative 53BP1 enhances HDR and inhibits NHEJ specifically at Cas9 target sites. Nat Commun. 2019;10(1):2866. [PubMed: 31253785]
57. Marciano BE, Zerbe CS, Falcone EL, Ding L, DeRavin SS, Daub J et al. X-linked carriers of chronic granulomatous disease: Illness, lyonization, and stability. J Allergy Clin Immunol. 2018;141(1):365–371. [PubMed: 28528201]
58. Rees HA, Yeh W-H, Liu DR. Development of hRad51–Cas9 nickase fusions that mediate HDR without double-stranded breaks. Nat Commun. 2019;10(1):2212. [PubMed: 31101808]
59. Nambiar TS, Billon P, Diedenhofen G, Hayward SB, Taglialatela A, Cai K et al. Stimulation of CRISPR-mediated homology-directed repair by an engineered RAD18 variant. Nat Commun. 2019;10(1):3395. [PubMed: 31363085]
60. Wienert B, Nguyen DN, Guenther A, Feng SJ, Locke MN, Wyman SK et al. Timed inhibition of CDC7 increases CRISPR-Cas9 mediated templated repair. Nat Commun. 2020;11(1):2109.
61. Frazão JB, Thain A, Zhu Z, Luengo M, Condino-Neto A, Newburger PE. Regulation of CYBB gene expression in human phagocytes by a distant upstream NF-κB binding site. J Cell Biochem. 2015;116(9):2008–2017. [PubMed: 25752509]
62. Roesler J, Brenner S, Bukovsky AA, Whiting-Theobald N, Dull T, Kelly M et al. Third-generation, self-inactivating gp91^{phox} lentivector corrects the oxidase defect in NOD/SCID mouse–repopulating peripheral blood–mobilized CD34^{+} cells from patients with X-linked chronic granulomatous disease. Blood. 2002;100(13):4381–4390. [PubMed: 12393624]
63. Pinder J, Salsman J, Dellaire G. Nuclear domain 'knock-in' screen for the evaluation and identification of small molecule enhancers of CRISPR-based genome editing. Nucleic Acids Res. 2015;43(19):9379–9392. [PubMed: 26429972]
64. Charpentier M, Khedher AHY, Menoret S, Brion A, Lamribet K, Dardillac E et al. CtIP fusion to Cas9 enhances transgene integration by homology-dependent repair. Nat Commun. 2018;9(1):1133. [PubMed: 29556040]
65. Ye L, Wang C, Hong L, Sun N, Chen D, Chen S et al. Programmable DNA repair with CRISPRa/i enhanced homology-directed repair efficiency with a single Cas9. Cell Discov. 2018;4(1):46. [PubMed: 30062046]
66. Lomova A, Clark D, Campo-Fernandez B, Flores-Bjurström C, Kaufman M, Fitz-Gibbon S et al. Improving gene editing outcomes in human hematopoietic stem and progenitor cells by temporal control of DNA repair. Stem Cells. 2018;37.
67. Yang D, Scavuzzo MA, Chmielowiec J, Sharp R, Bajic A, Borowiak M. Enrichment of G2/M cell cycle phase in human pluripotent stem cells enhances HDR-mediated gene repair with customizable endonucleases. Sci Rep. 2016;6(1):21264. [PubMed: 26887909]
68. Maruyama T, Dougan SK, Truttmann MC, Bilate AM, Ingram JR, Ploegh HL. Increasing the efficiency of precise genome editing with CRISPR-Cas9 by inhibition of nonhomologous end joining. Nat Biotechnol. 2015;33:538–542. [PubMed: 25798939]
69. Chu VT, Weber T, Wefers B, Wurst W, Sander S, Rajewsky K et al. Increasing the efficiency of homology-directed repair for CRISPR-Cas9-induced precise gene editing in mammalian cells. Nat Biotechnol. 2015;33:543–548. [PubMed: 25803306]
70. Robert F, Barbeau M, Éthier S, Dostie J, Pelletier J. Pharmacological inhibition of DNA-PK stimulates Cas9-mediated genome editing. Genome Med. 2015;7(1):93. [PubMed: 26307031]
71. Riesenberg S, Maricic T. Targeting repair pathways with small molecules increases precise genome editing in pluripotent stem cells. Nat Commun. 2018;9(1):2164–2164. [PubMed: 29867139]
72. Jayavaradhan R, Pillis DM, Malik P. A versatile tool for the quantification of CRISPR/Cas9-induced genome editing events in human hematopoietic cell lines and hematopoietic stem/progenitor cells. J Mol Biol. 2018;431.

73. Paulsen BS, Mandal PK, Frock RL, Boyraz B, Yadav R, Upadhyayula S et al. Ectopic expression of RAD52 and dn53BP1 improves homology-directed repair during CRISPR–Cas9 genome editing. Nat Biomed Eng. 2017;1(11):878–888. [PubMed: 31015609]

74. Cuella-Martin R, Oliveira C, Lockstone HE, Snellenberg S, Grolmusova N, Chapman JR. 53BP1 Integrates DNA Repair and p53-Dependent Cell Fate Decisions via Distinct Mechanisms. Mol Cell. 2016;64(1):51–64. [PubMed: 27546791]

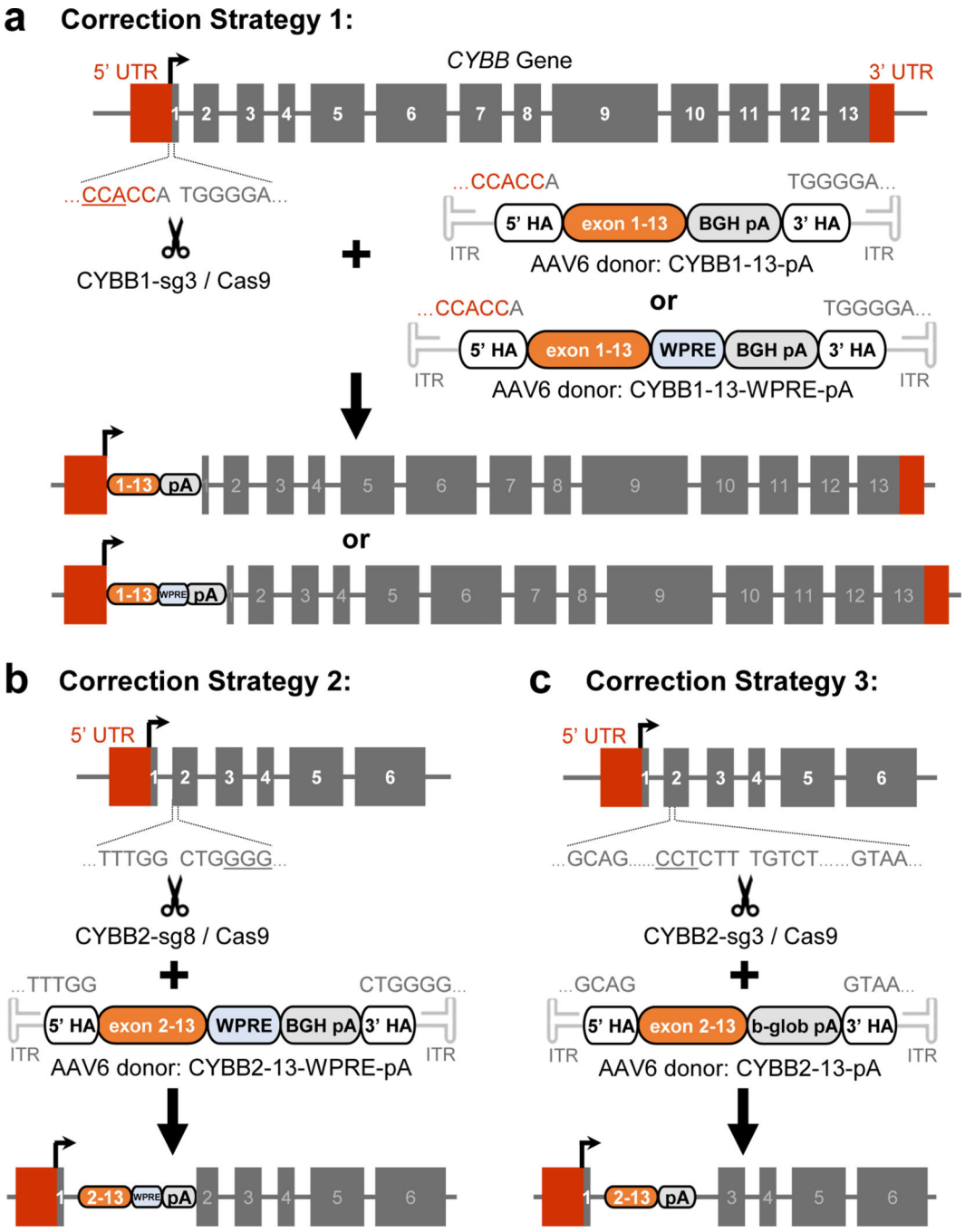

Fig. 1. Schemata of correction strategies for targeted *CYBB* cDNA insertion in X-CGD patient CD34$^+$ HSPCs.

(**a**) Strategy 1 utilizes CRISPR/Cas9 with CYBB1-sg3 sgRNA and an ~2.7-kb AAV6 donor template containing *CYBB* exon 1–13 cDNA and BGH poly-A signal (pA) for targeted insertion at *CYBB* exon 1 (CYBB1–13-pA); an alternative ~3.3-kb AAV6 donor contains a WPRE in addition to the exon 1–13 cDNA and BGH pA (CYBB1–13-WPRE-pA). (**b**) Strategy 2 utilizes CRISPR/Cas9 with CYBB2-sg8 sgRNA and an ~3.3-kb AAV6 donor template containing *CYBB* exon 2–13 cDNA with WPRE and BGH pA for targeted

insertion at exon 2 (CYBB2–13-WPRE-pA). (**c**) Strategy 3 utilizes CRISPR/Cas9 with CYBB2-sg3 sgRNA and an ~3-kb AAV6 donor template containing *CYBB* exon 2–13 cDNA with rabbit beta-globin (b-glob) pA for insertion at exon 2 (CYBB2–13-pA). Each donor template includes 5' and 3' homology arms (HA) of ~400-nucleotides each, flanking the cDNA expression cassette; the listed donor templates sizes do not include the sizes of the AAV ITRs required for viral packaging. Depicted for each strategy are the naive *CYBB* locus (top) including the CRISPR/Cas9 target site (with the PAM sequence underlined), the AAV6 donor construct (middle), and the *CYBB* locus after targeted insertion (bottom); for simplicity, only the first 6 exons of the *CYBB* locus are depicted for strategies 2 and 3.

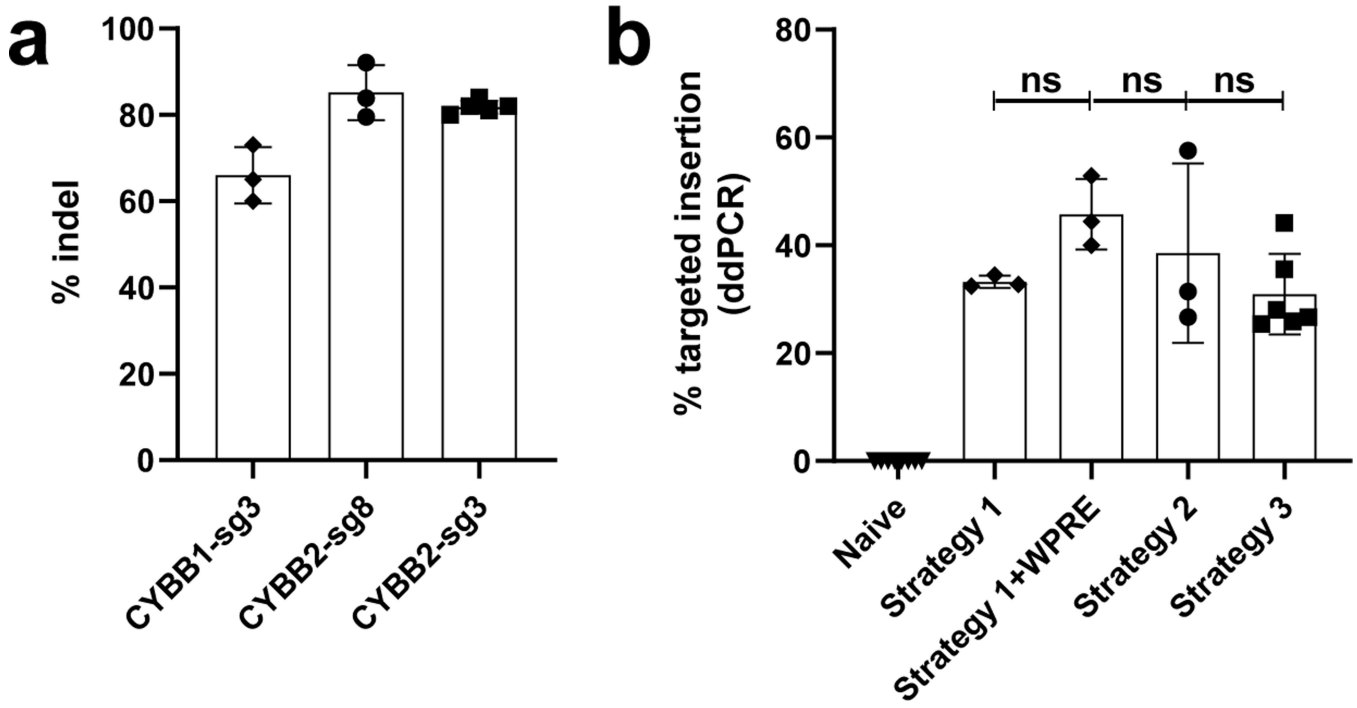

Fig. 2. Targeted genome editing efficiencies in HSPCs for correction strategies 1 through 3 using initial un-optimized editing conditions.

(**a**) Percent indel frequency by CRISPR/Cas9 using CYBB1-sg3 (strategy 1), CYBB2-sg8 (strategy 2), or CYBB2-sg3 (strategy 3) sgRNAs in male healthy donor or X-CGD patient HSPCs (bars denote mean ± SD; n = 3 for strategy 1 and strategy 2; n = 5 for strategy 3). (**b**) Targeted insertion frequency analysis by ddPCR in X-CGD patient HSPCs at 3–5 days after electroporation of CRISPR/Cas9 and transduction with AAV6 donor template (bars denote mean ± SD; n = 3 for strategy 1, strategy 1 +WPRE, and strategy 2; n = 6 for strategy 3; n = 8 for naive control; ns = not significant by one-way ANOVA with Tukey's multiple comparisons test).

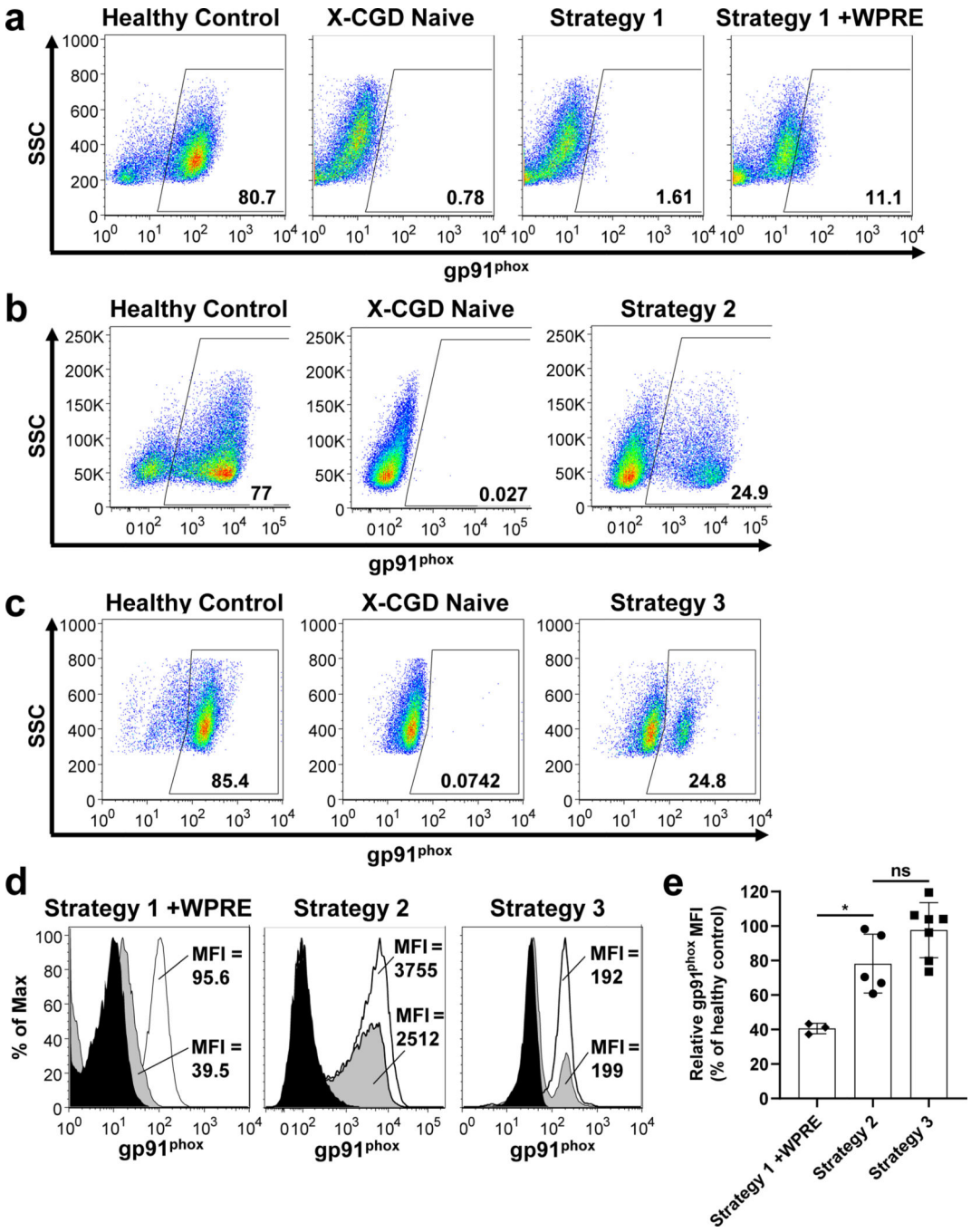

Fig. 3. Comparison of phenotypic correction of gp91^{phox} expression in differentiated phagocytes after targeted cDNA insertion in X-CGD HSPCs.

Shown are representative replicates of flow cytometry immunostaining analysis for cells corrected with (**a**) *CYBB* exon 1–13 cDNA with or without a WPRE for correction strategy 1 or strategy 1 +WPRE, (**b**) exon 2–13 cDNA with a WPRE for correction strategy 2, or (**c**) exon 2–13 cDNA for correction strategy 3. Y-axes represent side-scatter (SSC) measurements. Healthy donor controls and uncorrected X-CGD (X-CGD naive) patient controls are also shown. (**d**) Histogram overlays from representative replicate flow

cytometry analyses from (a-c) of per-cell levels of gp91^{phox} expression for strategy 1 +WPRE (left), strategy 2 (middle), or strategy 3 (right); black histogram = uncorrected X-CGD naive control; gray = corrected; white = healthy donor control; also shown are MFIs of the gated gp91^{phox+} cell populations for the corrected and healthy control phagocytes. (**e**) Summary of mean per-cell levels of gp91^{phox} expression in corrected cells for strategy 1 +WPRE, strategy 2, and strategy 3, calculated from flow cytometry analysis as the MFI of corrected cells relative to healthy controls for the gated gp91^{phox+} phagocyte populations (bars denote mean ± SD; n = 3 for strategy 1 +WPRE; n = 5 for strategy 2; n = 7 for strategy 3; *p<0.05 by one-way ANOVA with Tukey's multiple comparisons test; ns = not significant).

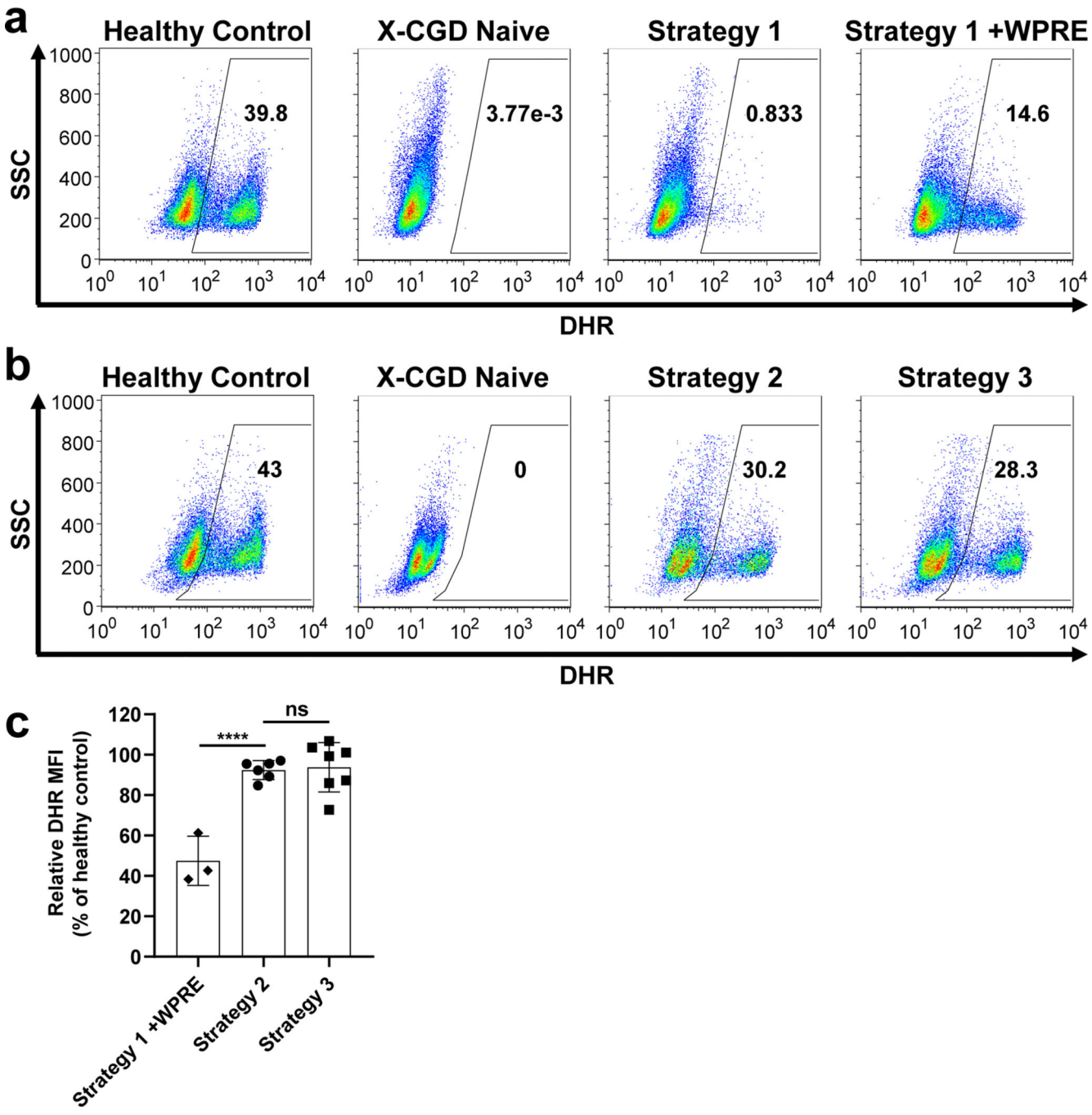

Fig. 4. Comparison of functional correction of ROS production measured by DHR assay in differentiated phagocytes after targeted cDNA insertion in X-CGD HSPCs.

Shown are representative replicates of DHR flow cytometry analyses for (**a**) strategy 1 +WPRE and (**b**) strategies 2 and 3, including healthy donor controls and uncorrected X-CGD (X-CGD naive) patient controls. (**c**) Summary of mean per-cell levels of ROS production in corrected cells for strategy 1 +WPRE, strategy 2, and strategy 3, calculated as the MFI of corrected cells relative to healthy controls for the gated DHR^{+} neutrophil populations (bars denote mean ± SD; n = 3 for strategy 1 +WPRE; n = 6 for strategy 2; n = 7

for strategy 3; ****p<0.0001 by one-way ANOVA with Tukey's multiple comparisons test; ns = not significant).

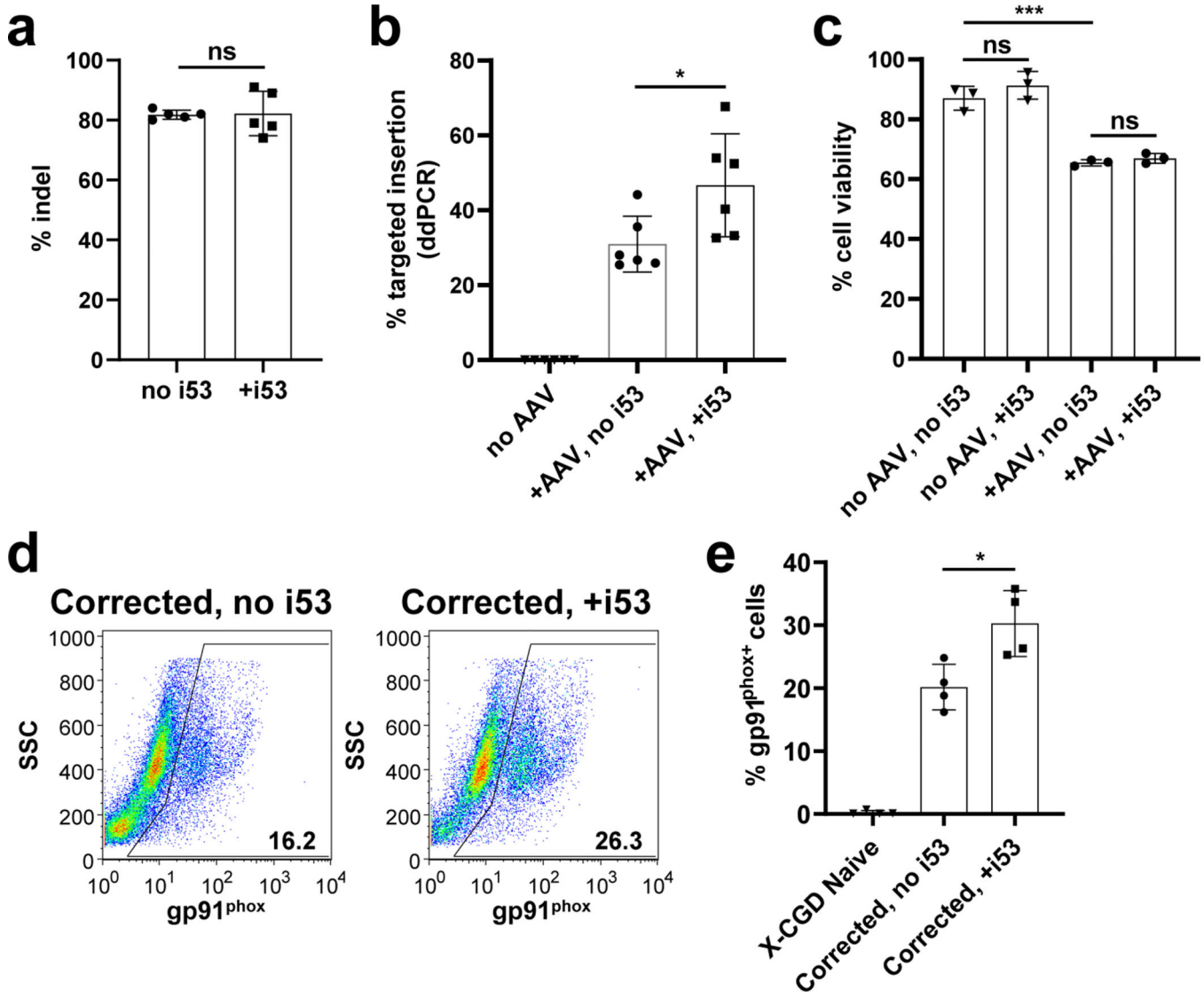

Fig. 5. Enhancement of targeted insertion efficiency using i53 mRNA in HSPCs with correction strategy 3.

(**a**) Percent indel frequency by ICE analysis in healthy donor HSPCs at 3–5 days after electroporation of Cas9 RNP with or without 48 pmol of i53 mRNA (bars denote mean ± SD; n = 5; ns = not significant by Wilcoxon matched-pairs test). (**b**) Targeted insertion frequency analysis by ddPCR in healthy donor HSPCs at 3–5 days after electroporation of Cas9 RNP (with or without 48 pmol of i53 mRNA) and transduction with AAV6 donor template at an MOI of 1×10^5 (bars denote mean ± SD; n = 6; *p<0.05 by Wilcoxon matched-pairs test). (**c**) Cell viability by trypan blue exclusion stain at 3 days after electroporation of Cas9 RNP with or without 48 pmol of i53 mRNA, and with or without AAV6 transduction at 1×10^5 MOI (bars denote mean ± SD; n = 3; ***p<0.001 by one-way ANOVA with Tukey's multiple comparisons test; ns = not significant). (**d**) Representative replicates from side-by-side comparisons of the effect of i53 mRNA co-transfection on correction of X-CGD patient HSPCs using AAV6 transduction at 1×10^5 MOI, analyzed by $gp91^{phox}$ expression following phagocyte differentiation. (**e**) Summary of the enhancement

by i53 mRNA (48–67 pmol) co-transfection on correction of X-CGD patient HSPCs by Cas9 RNP with AAV6 transduction at 1×10^5 MOI, analyzed by $gp91^{phox}$ expression following phagocyte differentiation (bars denote mean ± SD; n = 4; *$p<0.05$ by Mann-Whitney test).

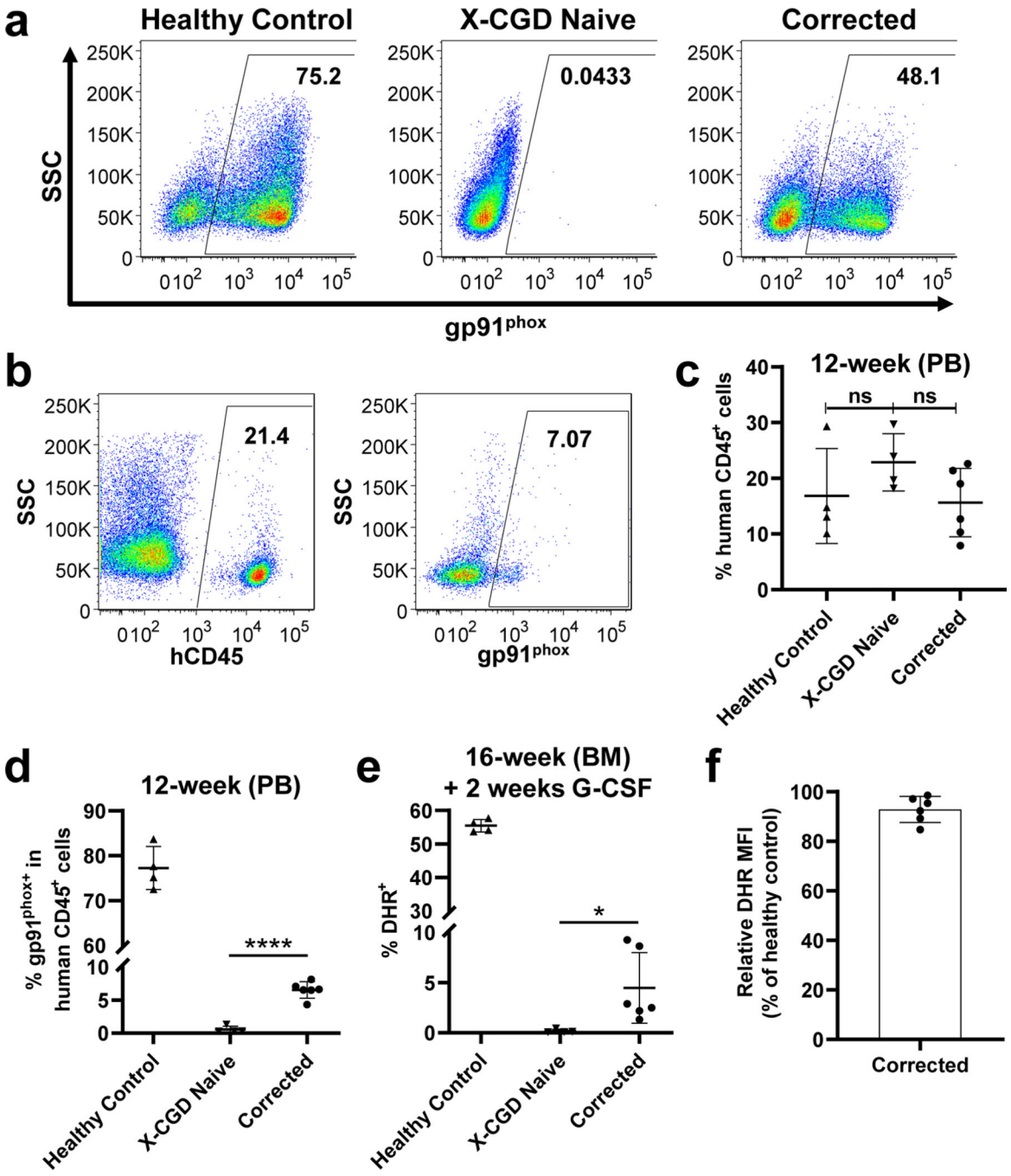

Fig. 6. Engraftment data of X-CGD patient HSPCs corrected using strategy 2 with optimized targeted insertion conditions and transplanted into NSG mice.

(**a**) *In vitro* data of the correction efficiency in the X-CGD patient HSPC population used for transplant, measured by gp91^{phox} expression in phagocytes following *in vitro* differentiation of untransplanted cells. (**b**) *In vivo* engraftment data from the peripheral blood of a representative mouse at 12 weeks post-transplant of corrected X-CGD HSPCs, immunostained for human CD45 (hCD45; left) as a marker of human hematopoietic cell engraftment and human gp91^{phox} (right; shown are gp91^{phox+} cells gated from the human

$CD45^+$ cell population) as a measure of corrected mature hematopoietic cells arising from engrafted human HSPCs. (**c**, **d**) Summary of (**c**) human $CD45^+$ cell engraftment in peripheral blood (PB) of NSG mice at 12 weeks post-transplant (bars denote mean ± SD; each replicate represents an individual transplanted mouse; n = 4 for healthy control and X-CGD naive HSPC transplants; n = 6 for corrected X-CGD HSPC transplants; ns = not significant by one-way ANOVA with Tukey's multiple comparisons test). (**d**) Summary of human $gp91^{phox+}$ cells gated from the human $CD45^+$ populations in PB at 12 weeks post-transplant (bars denote mean ± SD; each replicate represents an individual transplanted mouse; n = 4 for healthy control and X-CGD naive HSPC transplants; n = 6 for corrected X-CGD HSPC transplants; ****$p<0.0001$ by two-tailed unpaired Welch's t-test). (**e**) Human $CD34^+$ cells were harvested and sorted from mouse bone marrow (BM) at 16 weeks post-transplant and then differentiated for 2 weeks *in vitro* to generate mature phagocytes for DHR assay of ROS production as a measure of functional correction in engrafted $CD34^+$ HSPCs (bars denote mean ± SD; each replicate represents an individual transplanted mouse; n = 4 for healthy control and X-CGD naive; n = 6 for corrected X-CGD; *$p<0.05$ by two-tailed unpaired Welch's t-test). (**f**) Summary of mean per-cell levels of ROS production in gated DHR^+ corrected neutrophils from (e), calculated relative to healthy controls based on MFIs (bars denote mean ± SD; n = 6).